G. Giordano, A. Vona, T.O. Grillo, A. Frontoni, L. Calabrò, G. Carrasco-Núñez, A. Aiuppa, L. Caricchi, G. De Astis, D. Di Genova, G. La Spina, M. Piochi, M. Viccaro, R. Russo (2026) "Basaltic vulcanian paroxysmal eruptions: textural characteristics and eruption dynamics of the July 3rd, 2019, Stromboli eruption (Italy)", Volcanica, 9(1). doi: 10.30909/vol/iajq5592.

A gas-slug model for basaltic Vulcanian eruptions at open conduit volcanoes, constrained by textural characteristics and dynamics of the July 3rd, 2019, Stromboli eruption (Italy)

*G. Giordano,[1,2], A. Vona[1], T.O. Grillo[1], A. Frontoni[1,2], L. Calabrò[3], G. Carrasco-Núñez[4], A. Aiuppa[5], L. Caricchi[6], G. De Astis[7], D. Di Genova[3], G. La Spina[8], M. Piochi[9], M. Viccaro[10], R. Russo[1]

[1] Dipartimento di Scienze – Scienze Geologiche, Università Roma Tre, Largo San Leonardo Murialdo 1, 00146, Rome, Italy

[2] Istituto di Geologia Ambientale e Geoingegneria del Consiglio Nazionale delle Ricerche, Montelibretti, Italy

[3] Istituto di Scienza, Tecnologia e Sostenibilità per lo sviluppo dei Materiali Ceramici, Consiglio Nazionale delle Ricerche, Via Granarolo, 64, 48018 Faenza RA

[4] Instituto de Geociencias, Universidad Nacional Autónoma de México, Campus UNAM Juriquilla, 76100, Querétaro, Mexico

[5] Dipartimento di Scienze della Terra e del Mare, Università di Palermo, Palermo, Italy.

[6] Department of Earth Sciences, University of Geneva, Geneva, Switzerland

[7] Istituto Nazionale di Geofisica e Vulcanologia, Via di Vigna Murata 605, 00143, Rome, Italy

[8] Istituto Nazionale di Geofisica e Vulcanologia- Osservatorio Etneo, Catania, Italy

[9] Istituto Nazionale di Geofisica e Vulcanologia – Osservatorio Vesuviano, Napoli, Italy

[10] Dipartimento di Scienze Biologiche, Geologiche e Ambientali, Università degli Studi di Catania, Corso Italia 57, 95129 Catania, Italy

*corresponding author: guido.giordano@uniroma3.it

Abstract

Stromboli is a unique open-conduit mafic volcano known for persistent Strombolian eruptions of highly porphyritic (HP) basaltic-shoshonite scoria. Stronger paroxysmal explosions occur once or twice per decade, ejecting low porphyritic (LP) golden pumice from deeper volatile-rich magma. The July 3rd, 2019, paroxysm showed features of a Vulcanian eruption - supersonic blast, ballistic ejection, and pyroclastic flows - despite Stromboli's open-conduit basaltic nature. Textural analysis suggests that LP pyroclasts formed via rapid decompression, fragmentation, and quenching. This event likely resulted from shallow HP-filled conduit pressurization and failure triggered by a rising large gas slug. This caused top-down decompression, evacuating both HP and deeper LP magma. The proposed "basaltic Vulcanian" model better fits geophysical data than the traditional deep LP magma ascent model.

KEYWORDS: Stromboli; Explosive eruption; Eruption dynamics; Paroxysm; Basaltic Vulcanian eruption style; Open conduit; Gas slug

1 Introduction

Vulcanian eruptions represent the sudden release of overpressure stored at the base of a viscous and degassed crystal- and bubble-bearing magma plug filling the conduit at shallow depths (Self et al., 1978; Clarke et al., 2015). The term "Vulcanian" takes from the original observations of the 1888-1890 latite-rhyolite eruption at Vulcano in the Aeolian volcanic arc (Mercalli and Silvestri, 1891). Since then, the Vulcanian eruption style has been extended worldwide and is typical of intermediate to felsic volcanoes. According to Clarke et al. (2015), some of the most common observational characteristics of Vulcanian eruptions are (i) the relatively small magnitude (Volcanic Explosivity Index ≤3-4); (ii) the release of initial shock waves followed by a typical mushroom-shaped jet feeding a short-lived plume ≤10 km high; (iii) the relatively small-sized ejecta associated with strong vent clearing ballistic ejection; (iv) the highly variable vesicularity of pyroclasts. Collectively, these characteristics point to a mechanism of pressurization and sudden decompression-driven fragmentation due to the failure of a shallow viscous magma plug or dome (e.g. Turcotte et al., 1990; Woods, 1995; Clarke et al., 2002, Kennedy et al., 2005). Giordano and De Astis (2021) have described the

observed eruption style of the two sudden explosive eruptions occurred in 2019 at Stromboli volcano (cf. i, ii) and the associated deposit types (cf. iii, iv), including the occurrence of pyroclastic flows, discussing in detail how these match with a Vulcanian eruption style (cf. Giordano et al., 2024), and proposed the new category of "basaltic Vulcanian eruptions" to indicate such unusual eruption style for an open conduit basaltic volcano.

This interpretation questions the common and exclusive association of Vulcanian eruptions with intermediate to felsic volcanoes and perhaps justifies why the scientific community has been so far very hesitant in assigning an eruption style to sudden, impulsive, and vent-clearing eruptions at Stromboli, with few exceptions (e.g. Calvari et al., 2006; Di Lieto et al., 2020). Instead of Vulcanian, the term "paroxysm" was initially proposed at Stromboli for such kinds of eruptions (Barberi et al., 1993), but only as a local operational term relative to the scale of observed explosive intensities (Imbò, 1930; Abbruzzese, 1935). However, since then, the term has spread worldwide without a definite connotation, so it is now associated with a plethora of different small-volume explosive eruption styles mostly defining the most violent phases at persistently to semi-persistently mafic volcanoes that include also classic fire fountaining, classic cone-forming violent Strombolian eruptions, such as at Etna volcano (e.g. Giuffrida et al., 2023 and references therein), along with eruptions with less defined styles (e.g. Taddeucci et al., 2015; c.f. Cashman and Sheu, 2015). The main commonality, though, is that all these different types of "paroxysms" at mafic volcanoes, including at Stromboli, are mostly interpreted as due to the rapid ascent of fresh, volatile rich, deep-seated magma through the conduit, so that vesiculation is associated with a classic bottom-up decompression mechanism and a dominantly inertial fragmentation (e.g. Namiki and Manga, 2008; Gonnermann et al., 2013). Such conduit processes also include degassing-induced crystallization upon magma ascent, able to significantly increase basaltic magma viscosity, allowing variable degrees of kinetic coupling between rising magma and bubbles, in turn controlling the intensity of the explosive eruption (e.g. Houghton and Gonnermann 2008).

The nearly aphyric LP magma erupted during the so-called "paroxysms" at Stromboli (Bertagnini et al., 2003, 2011; Métrich et al., 2005, 2010, 2021; Pichavant et al., 2009, 2022; Pioli et al., 2014; Landi et al., 2022) constitutes a significant outlier in this scheme as, different from other occurrences (e.g. Gurioli et al., 2008), it forms highly fragmented aphyric pumice with structure that closely resembles felsic pumice, allowing it to float as lapilli rafts for weeks or longer after such explosive events (Giordano and De Astis, 2021).

In this paper we explore what the texture of basaltic-shoshonite LP pyroclasts of the July 3rd, 2019, explosive eruption at Stromboli can tell us about the associated eruption style. We ground our interpretations in a thorough review of existing conceptual models for large scale explosions at Stromboli. We aim to clarify whether and under what conditions Vulcanian eruptions can occur at Stromboli and possibly at other open conduit basaltic volcanoes.

1.1 Overview of Stromboli volcano eruption styles and a summary of the July 3rd, 2019, eruption

Stromboli is an open conduit basaltic-shoshonitic volcano characterized by recurrent small explosions of spatter and scoria, forming sprays a few tens to a few hundred meters in height from a crater terrace located at 750 m a.s.l. (now significantly modified and lowered after the July 2024 eruption; Civico et al., 2024), within the Sciara del Fuoco collapse scar, associated with the Holocene collapses of the volcano edifice (Fig. 1a; Lucchi et al., 2013; Vezzoli and Corazzato 2016). This type of persistent activity gives name to the Strombolian eruption style *sensu stricto* (Giordano et al., 2024) and is considered "ordinary", occurring on average every few minutes to a few tens of minutes (Barberi et al., 1993; Ripepe et al., 1993; Harris and Ripepe 2007; Patrick et al., 2007; Leduc et al., 2015; Calvari et al. 2021). Occasionally, Stromboli exhibits other eruption styles, including effusive activity or more intense explosions called "major" and "paroxysmal". Major and paroxysmal eruptions form short-lived plumes, with the largest reaching several kilometers in height, and are associated with the launching of ballistics well across the rim of the collapse scar, potentially reaching the touristic and settled areas (Barberi et al., 1993; Bevilacqua et al., 2020) also setting wildfires (Turchi et al., 2020, Guardo et al., 2024; Iacono et al., 2025). Furthermore, they can also generate small pyroclastic currents that flow down to the sea and spread over its surface, triggering tsunamis (Bertagnini et al., 2011; Bevilacqua et al., 2020; Esposti Ongaro et al., 2021; Ripepe and Lacanna, 2024). Paroxysmal events are relatively infrequent, with 36 events recoded in the last 140 years (Bevilacqua et al., 2020); in this century they occurred in 2003, 2007, two in 2019, and in 2024, with mass eruption rates calculated in the order of 10^6-10^7 kg s^{-1} (Pistolesi et al., 2008, 2011; Giordano and De Astis 2021; Andronico et al., 2021). The July 3rd, 2019, eruption (Fig. 2a) is one of the largest of these paroxysmal events (Giudicepietro et al., 2020; Viccaro et al., 2021; Giordano and De Astis, 2021; Andronico et al., 2021; Calvari et al. 2021). The paroxysmal eruption was not forecasted, as it occurred unexpectedly at 14:45 UTC, without any issued

warning. Different from previous events, the eruption occurred during a period of ordinary activity characterized by Strombolian explosions (Giudicepietro et al., 2020). The only signal recognized at that time as precursor was the short-term, sudden acceleration and increased amplitude of the ground deformation initiated only about ten minutes prior to the eruption (Di Lieto et al., 2020; Giudicepietro et al., 2020; Viccaro et al., 2021; Mattia et al., 2021; Ripepe et al., 2021). This eruption caused one victim, caught in the bushfires triggered along the volcano flank, but the toll could have been much higher, as it took place just a few hours before hundreds of tourists were expected to reach the summit of the volcano to observe the ordinary Strombolian explosions. Since then, the summit of Stromboli volcano has been closed to tourism.

The explosive eruption initiated with acoustic shock waves at the front of a rapidly and radially expanding blast (Fig. 1a,b) with finger-jets made of ballistic lava lithics and highly porphyritic (HP) spatter clasts that entirely covered the summit area (Fig. 1c). Pyroclastic flows were generated along the Sciara del Fuoco. After about 12 seconds a vertical buoyant plume started to form (Fig. 1d). The plume rose to a maximum height of 8.4 km, then spread laterally toward the SW depositing a thin blanket of low porphyritic (LP) pumice lapilli (Fig. 1c). The eruption was fed for about 5 minutes. Table 1 reports the main observational and physical characteristics of the July 3rd, 2019 eruption and its deposits.

Magma composition	basaltic shoshonite
Eruption Duration	5 min
Style	blast/shock waves
Vent shape	destructional crater (~70 m)
Jet shape	overpressured bulb
Jet height (km)	>0.5
Ballistic max exit velocity (m s^{-1})	120-160
Jet exit velocity (m s^{-1})	220-250*
Average plume rise velocity in the 1st km (m s^{-1})	100
Plume maximum height (km)	8.4
Pumice fall duration (min)	35-45
Pyroclastic density currents	yes
Mass eruption rate (kg s^{-1})	1.1 x 10^6
Volume of the summit total spatter cover (m^3)	1.05 x 10^5
Volume of the summit HP spatter cover (m^3)	7 x 10^4
Mass of summit total spatter cover (kg @ $\rho_{spatter}$=1350 kg m^{-3})	1.4 x 10^8
Mass of the summit HP spatter cover (kg)	7 x 10^7
Max thickness of continuous spatter cover (cm)	35-40

5 cm isopleth area (km^2)	4
Pumice fall dispersal axis	SW

Table 1 - Summary of Stromboli July 3rd, 2019, Vulcanian paroxysm characteristics (data from Giordano and De Astis, 2021, and *Andronico et al., 2021)

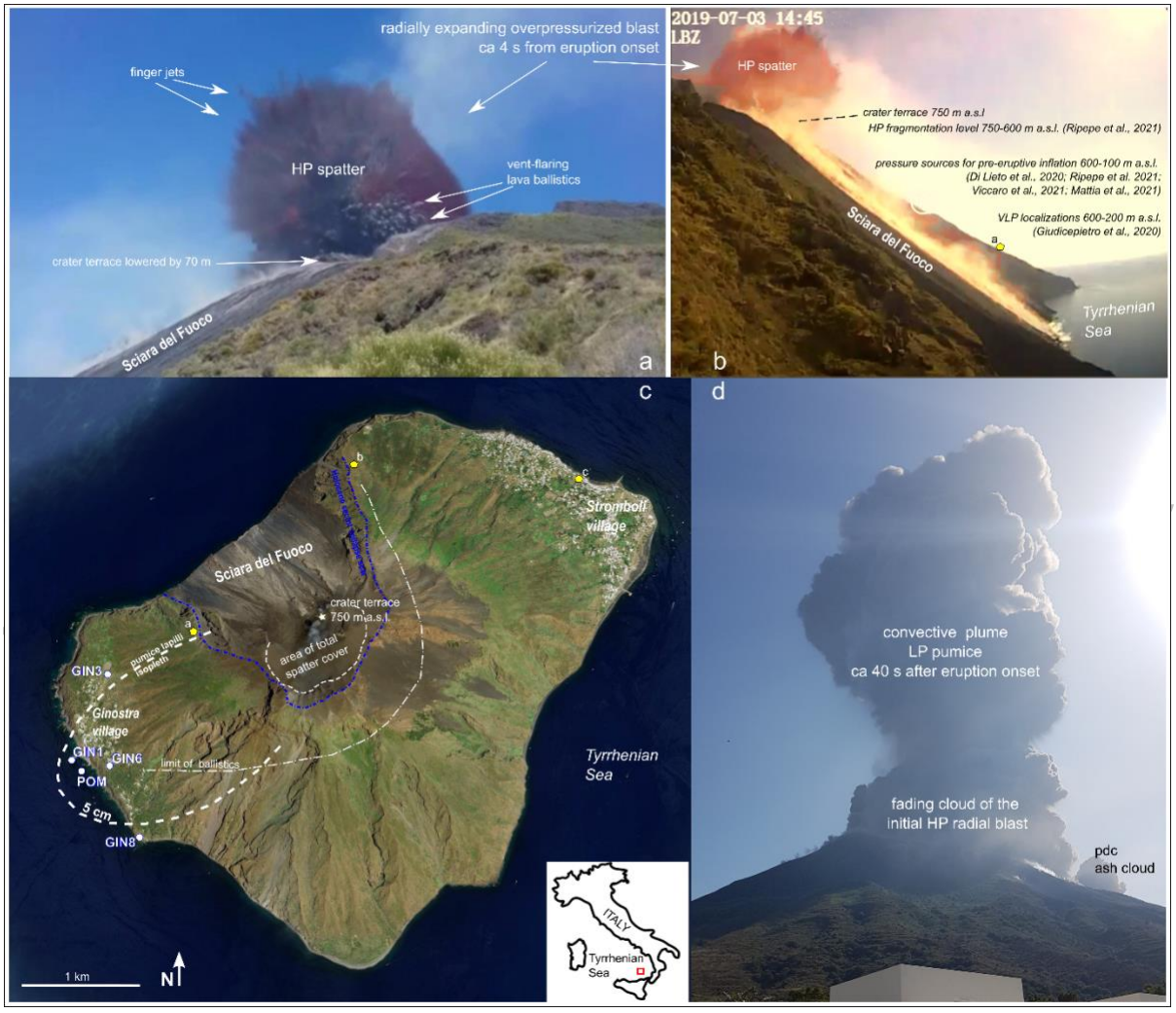

Fig. 1 – a,b) Views of the initial blast from the two sides of the Sciara del Fuoco (a – frame from a video taken by Thiago Takeuti from the Ginostra side; b - image from the videorecord of the LBZ monitoring camera, courtesy of Laboratorio di Geofisica Sperimentale, Università di Firenze; see Fig. 1c for location; the yellow symbol in Fig.1b indicates the approximate viewpoint for the image in Fig. 1a); the eruption started forming a bulb that radially expanded for a few seconds forming finger-jets, breaching and lowering the vent by 70 m and launching m-sized spatter and lithic ballistics almost radially, with a preferential direction toward the sea. The expanding

bulb was made entirely by HP-magma spatters that formed a 30-40 cm thick cover in the summit area (Fig. 1c). The blast was then followed, after ca. 12 seconds from eruption start, by the rise of a buoyant plume (Fig. 1d) (see Giordano and De Astis, 2021 for details). The approximate elevation of the fragmentation level and pressurization sources along with VLP seismicity that anticipated the event are indicated in (b). See text for explanation.

c) The volcanic island of Stromboli (satellite image from GoogleEarth). The July 3rd, 2019, Vulcanian eruption originated from the crater terrace, located inside the Holocene Sciara del Fuoco collapse scar (dashed blue line). The limit and the area of total spatter cover (white thin dashed line; dominated by HP spatter), the limit of ballistics (dash-and-dotted white line) and the 5 cm isopleth of pumice lapilli (white thick dashed line; dominated by LP pumice) are taken from Giordano and De Astis (2021). The Sciara del Fuoco collapse scar (blue dashed line) shelters the two main villages of Stromboli and Ginostra from the ordinary activity but not from the occasional more intense explosive eruptions. Sampling localities GIN1 (Lat 38°47'07.22"N; Lat 15°11'21.81"E), GIN3 (Lat 38°47'29.86"N; Lat 15°11'32.14"E), GIN6 (Lat 38°47'06.66"N; Lat 15°11'34.25"E), GIN8 (Lat 38°46'47.84"N; Lat 15°11'47.13"E) and POM (Lat 38°47'07.40"N; Lat 15°11'24.49"E) for textural analyses are also indicated. The yellow symbols indicate the locations from where photos a), b) and d) were taken.

d) Volcanic plume of the July 3rd, 2019, Stromboli eruption, about 40 seconds after its onset, seen from the Stromboli village (see Fig. 1c for location); at the base it is possible to see the fading of the initial radial blast that fed pyroclastic flows (pdc) along the Sciara del Fuoco (note the associated ash cloud rising to the right of the main plume); the convective region of the plume later rose to a maximum height of 8.4 km feeding a laterally spreading umbrella from which the LP pumice lapilli fell out onto the Ginostra village for approximately 35 minutes.

1.2 State of the art of existing conceptual models for sudden large explosions (paroxysms) at Stromboli

One of the common characteristics of the Stromboli so-called "paroxysms" is the emptying of the shallow portion of the open conduit, which is persistently filled by highly crystallized and degassed, almost ponding magma, known in the literature as highly porphyritic (HP) magma. This HP magma bears 45-55 vol% of crystals (plagioclase, clinopyroxene and olivine; Bertagnini et al., 2008; Lautze and Houghton 2005; Métrich et al., 2010) and forms dark scoria during the ordinary Strombolian activity and lava during effusive events (Landi et al., 2006, 2009). Along with the HP magma, a fresh, pale and almost aphyric magma, known as low porphyritic (LP) magma with1-10 vol% of crystals (clinopyroxene and olivine; Bertagnini et al., 2011; Métrich et al., 2021; Pichavant et al., 2022), is erupted in all paroxysms, producing highly vesicular golden pumice.

The LP magma belongs to the deeper parts of the plumbing systems and according to experiments originates at pressures of 150-200 MPa (Di Carlo et al., 2006; Pichavant et al., 2009, 2011) or of 210 MPa, which account for the total volatile content measured in olivine-hosted melt inclusions (Métrich et al., 2010). These pressures correspond to depths of 7-10 km, with recharge coming from deeper levels (P~280 MPa; Métrich et al., 2010).

According to decompression experiments, the transition from LP to HP magma is thought to occur at depths comprised between 2 and 4 km, where CO_2 flushing drives H_2O exsolution from the persistently recharged LP magma, allowing plagioclase crystallization (Métrich et al., 2010, 2021 Pichavant et al., 2009, 2022; Patané et al., 2017; Landi et al., 2022). At such depths dynamic mixing and mingling of HP and LP magmas are envisaged, allowing the formation of hybrid compositions (Landi et al., 2022).

There is consensus on the primary role of the very fast rise of small batches of gas-rich LP magma (magma batch volumes of 10^3-10^5 m^3, Bertagnini et al., 2003) from the 7-10 km reservoir as the trigger for paroxysmal events, although the exact mechanisms are still matter of debate (Bertagnini et al., 2003, 2011; Calvari et al., 2006, 2021; Rosi et al., 2006; Landi et al., 2009, 2022; Pichavant et al., 2009, 2022; Métrich et al., 2010, 2021; Aiuppa et al., 2021; La Spina et al., 2015; Caricchi et al., 2024; Stix et al. 2025).

Petrologic data for the July 3rd, 2019, event record timescales of hundreds to a few days for repeated events of recharge of the deep LP magma before paroxysms (Métrich et al., 2021; Petrone et al., 2022). These data also reveal the progressive ascent of small batches of LP magma into the base of the HP magma, with evidence of mingling and mixing between the two (Métrich et al., 2021; Pichavant et al., 2022; Landi et al., 2022), potentially contributing to a transient shallowing of the HP-LP transition.

These inferred timescales match those indicated by the progressive increase in CO_2 flux measured in the volcanic plume during the months preceding the 2019 paroxysm (Aiuppa et al., 2021; Caricchi et al., 2024; Stix et al. 2025), the rise in very long period (VLP) seismicity and ordinary explosions frequencies (Mattia et al., 2021; Calvari et al. 2021), as well as seismic, infrasonic and deformation patterns (Di Traglia et al. 2021; Giudicepietro et al., 2022). Caricchi et al. (2024) suggested that CO_2 flushing at the base of the magmatic column over timescales of months may induce H_2O degassing and the development over time of a layer of bubble-rich LP magma. The progressive increase of gravitational instability would eventually result in the

repeated rise of batches of LP magma toward the shallower portions of the conduit, building up conditions for paroxysms and/or other non-ordinary eruption styles, including effusive (Laiolo et al., 2022).

The withdrawal of critical volumes of magma during the effusive eruptions, that preceded the 2003 and 2007 paroxysms, were suggested as possible triggers for the decompression and sudden and fast rise of deep-seated LP magma leading to the paroxysms (Bonaccorso et al., 2008; Landi et al., 2009; Laiolo et al., 2022). This phenomenological pattern could be applied to some extent to the sequence of events that preceded the July 2024 eruption (Civico et al., 2024). However, this interpretation cannot account for the sudden occurrence of paroxysms during ordinary Strombolian activity, as was the case with the July 3rd, 2019, event (Giudicepietro et al 2020; Giordano and De Astis, 2021; Viccaro et al., 2021).

Based on olivine growth calculations (Bertagnini et al., 2003) and plagioclase reaction rims (Pichavant et al., 2022), timescales for the rise of a batch of LP magma that is supposed to trigger paroxysms have been estimated at hours to tens of hours and velocities of 1-2 m s^{-1} from depths of 7-8 km. In contrast, based on Fe-Mg diffusion profiles in olivine and clinopyroxene, Métrich et al. (2021) suggested final ascent rates of days. Mattia et al. (2021) envisaged, instead, the LP magma as a water-melt solution made by 70% of supercritical exsolved water rising from the LP-HP transition boundary.

Based on experimental constraints, Valdivia et al. (2023) recently proposed that the viscosity of Stromboli LP magma is lower than previously estimated (Misiti et al., 2009; Giordano et al., 2009; Langhammer et al., 2022). Under pre-eruptive conditions (T = 1150 °C, H_2O = 3.67 wt%, and free of CO_2), Valdivia et al. (2023) found that the Stromboli melt viscosity is < $\log_{10}$ 10^1. Using a simple ascent rate model that neglects the shear-rate dependence of viscosity (Kokandakar et al., 2018), the authors determined the ascent velocity of a bubble-free Stromboli basalt. With a crystal content of 10 vol%, the velocity of magma ascending through a 4 m wide dike was calculated to be 41 m s^{-1}, approximately 30% faster than previously estimated (Misiti et al., 2009). Such high velocity is broadly consistent with independent estimates derived from pre-explosion ground deformation analyses by Ripepe et al. (2021)..

Irrespective of the depth and timing of the LP magma batch upward migration, the trigger for paroxysmal explosions is commonly attributed to its momentum and expansion, thought to push, displace and perch through the shallow ponding and more viscous HP magma (Métrich

et al., 2010, 2021; Bertagnini et al 2011; Pichavant et al., 2022; Aiuppa et al., 2021; Mattia et al., 2021; Ripepe et al., 2021; Di Traglia et al. 2021).

The trigger models for paroxysmal events at Stromboli summarized above and referred from here onwards as the "standard model" (also called "magma blob model" by Pichavant et al., 2022), involve the rapid ascent of a gas-rich batch of deep-seated magma in a two-phase closed-degassing system (bubbly flow; Vergniolle and Gaudemer, 2015). These models are similar to those commonly invoked for basaltic fire fountaining (e.g. Mangan and Cashman 1996, Polacci et al., 2006; Mangan et al., 2014; Holt et al., 2019) and violent Strombolian eruptions (e.g. Pioli et al., 2008; Cimarelli et al., 2010; Taddeucci et al., 2015). However, the resulting eruption style at Stromboli is fundamentally different (Fig. 1; Giordano and De Astis, 2021). In addition, paroxysmal events at Stromboli are distinctive in producing aphyric pumice clasts that dominate the deposits from the buoyant plume. This contrasts with the common microlite-rich scoria product erupted in the other mild explosive basaltic eruption styles (e.g. Taddeucci et al., 2004; Gurioli et al., 2008; Johnson et al., 2008). The almost total absence of microlites in the LP pumice implies that degassing-induced crystallization did not take place in the LP magma during ascent (Bertagnini et al., 2003; Métrich et al., 2010; Andronico et al., 2021; Pichavant et al., 2022). This observation challenges the commonly observed positive relationship between crystallinity and explosivity of basaltic magmas (e.g. Houghton and Gonnermann 2008; Caricchi et al., 2018). To explain the lack of microlites, Di Carlo et al. (2006) and Pichavant et al. (2022) proposed an adiabatic ascent path for the LP magma, ignoring the possible presence of free fluid phase, which is very unlikely in the Stromboli open system. Other hypotheses include the buoyant rise of bubbly LP magma driven by the flushing of CO_2 in the deep plumbing system, which delays water exsolution and crystallization until shallow levels (Métrich et al., 2005; Di Carlo et al., 2006; Caricchi et al., 2024). The magma ascent should occur under strong disequilibrium conditions, induced by high ascent velocity (e.g., La Spina et al., 2016; Polacci et al., 2018; Arzilli et al., 2019).

An alternative to the "standard model" is the "gas slug model" proposed by Allard (2010). This model suggests that paroxysms are triggered by the rise of gas slugs that separate from the melt through a process known as foam collapse (Jaupart and Vergnoille, 1989). This process should be preceded by the formation of the foam by gas accumulation, particularly at geometric kinks of the plumbing system (Chouet et al., 2008; Aiuppa et al., 2011, 2021), or at rheological barriers (Caricchi et al., 2024). Viccaro et al. (2021) demonstrated very short Li diffusion

timescales in plagioclase, suggesting that conduit geometry plays a role in slowing gas slug percolation through the very shallow HP conduit. This process leads to conduit pressurization and failure, with the resulting LP eruption interpreted as a passive decompression-driven discharge. Additionally, Visalli et al. (2023) highlighted significant small-scale compositional heterogeneities in the residual glasses of both HP and LP fragments. These heterogeneities are attributed to the short-term hybridization between the two magma end members that occurred shortly before the eruption (cf. Landi et al., 2022).

Whatever the actual trigger of paroxysms at Stromboli, several authors (e.g. Métrich et al., 2010; Aiuppa et al., 2021; Pichavant et al., 2022) have acknowledged the difference between petrological and geochemical timescales, which extend from months to hours, and geophysical signals such as edifice inflation, which occur, as unequivocal precursors, just a few minutes before the eruption and point to very shallow pressure sources (Di Lieto et al., 2020; Giudicepietro et al., 2020, 2022; Di Traglia et al. 2021 Mattia et al., 2021; Ripepe et al., 2021; Viccaro et al., 2021).

In summary the mechanisms driving paroxysmal explosions at Stromboli remain poorly understood and may differ fundamentally from those associated with other explosive eruption styles at basaltic volcanoes.

2 Materials and Methods

Grain-size, density and textural analyses were performed on July 3rd, 2019, LP pumice clasts to investigate the conduit dynamics of the LP magma, as it is indicated as the potential trigger for paroxysms. Samples were collected on a 40 cm x 40 cm surface along the southeastern flank of the volcano (GIN1, GIN3, GIN6 and GIN8 sites in Fig. 1; Giordano and De Astis 2021) and represent the dispersal of the pumice fallout from the convective and umbrella region of the plume (Giordano and De Astis, 2021; Andronico et al., 2021; Métrich et al., 2021). These LP pumice samples refer to the phase of the eruption that immediately followed the initial overpressurized blast that emplaced the ballistic spatter cover of HP magma at the summit (Fig. 1; Giordano and De Astis, 2021; Bisson et al., 2023), and are considered to quench the conditions of the deep magma system. The HP textures are instead significantly modified after fragmentation, and do not provide information on conduit processes, hence have not been investigated. In addition, one LP ballistic bomb was taken at site GIN3 (OST1), as well as

floating pumice clasts (POM) taken from rafts in the Ginostra offshore (Fig. 1). The density of LP pumice lapilli has been measured with a hydrostatic balance on 59 clasts (GIN1 n=21; GIN6 n=16; GIN8 n=17; POM n=5) according to Houghton and Wilson (1989). These clasts were selected to encompass the macroscopic variability in terms of morphology, colour and vesicularity. At GIN1, GIN6 and GIN8 sampling sites, twelve LP pumice clasts were selected for textural analyses from the grain size classes >16mm, >8mm and >4mm that form the coarse fraction around the mode of the grain size distribution (Supplementary material SM1). As the mode of the grain size ranges between 2 and 4 mm, the choice of grain sizes around and coarser than the mode has been considered a good compromise to represent the most frequent grain sizes, also in view of the scarcity or absence of larger clasts (Supplementary Material SM1). This choice also allowed to select clasts in the lapilli range that include large vesicles (unlike the previous textural studies by Andronico et al., 2021 and by Pichavant et al., 2022 on ash clasts of the same deposit), and at the same time small enough to have fast quenched in air remaining unaffected by significant post-fragmentation modifications (cf. Andronico et al., 2021). Images at different magnifications (60x, 120x, 240x, and 480x; minimum pixel size of 0.5 microns) have been acquired with a Zeiss Sigma 300 Field Emission Scanning Electron Microscope (FE-SEM) equipped with a 40-XMAX^N micro-analysis system by Oxford, controlled by SMARTSEM 5.09© and AZTEC 3.0© softwares (INGV-Osservatorio Vesuviano; Department of Science for morphological analyses, at University Roma Tre for acquisition of thin section images). Operating conditions were 10-to-20 kV accelerating voltage, 50–100mA filament current, 5–10 nm spot size and variable acquisition time (several to tens of seconds). For each clast, an area between 12.66 and 22.86 mm^2 has been analyzed (Table 2). Vesicle population in acquired images was manually outlined and binarized using the ImageJ software (imagej.nih.gov/ij/). Subsequently, FOAMS Matlab code (Shea et al., 2010) has been used to process and evaluate textural features, such as shape, size distributions, and Vesicle Number Density (VND). Sample GIN3 has been analysed by 3D X-ray microtomography acquired with a Zeiss XRadia Versa 510 (Universidad Nacional Autonoma de Mexico) and processed with the software Avizo 3D 2020.1 in order to avoid border effects on volumes of 600x600x600 voxels.

3 Results

3.1 Clast morphology and qualitative textural observations

The juvenile population of the analysed samples is dominated by LP and mingled LP-HP pumice clasts (Supplementary Material SM2), with crystal content <10 vol% and variable vesicle content (Fig. 2a,b). The chemical composition is basaltic shoshonite, as determined by previous studies (Andronico et al., 2021; Viccaro et al., 2021; Pichavant et al., 2022). Pumice lapilli clasts (GIN1, GIN3, GIN6, GIN8, POM) are yellowish to pale brown and angular to subangular in shape (Fig. 2b). The external surfaces vary from sharp planes, evidence of quenched brittle fragmentation, to variably irregular, with evidence of some post-fragmentation melt relaxation. Vesicularity appears rather homogeneous forming a foam of well-packed sub-millimetric rounded vesicles that are cut by the external surface (Fig. 2c,d). Larger mm-sized vesicles are scattered and form a distinct population with their floor made of relaxed glass surface paved by smaller rounded vesicles (Fig. 2c,d). The most abundant small size vesicle population is made of spherical vesicles isolated to incipiently coalesced with no evidence of post-coalescence melt relaxation (Fig. 2e,f). The overall shape of the larger vesicles is not significantly deformed by the growth of the smaller ones, suggesting synchronous growth for all sizes before quenching (Fig. 2c,d,).

No significant macroscopic difference in shape and vesicularity are observed between pumice lapilli from the fallout collected on the island (GIN1, GIN3, GIN6, GIN8) and those collected from the floating pumice raft (POM). Bombs (OST1) show mingled HP and LP domains with evidence of post-fragmentation growth of large bubbles in their interior (Fig. 2a).

The described compositional and morphological features are comparable with LP pumice textural characterization from previous paroxysmal events (cf. Métrich et al., 2001, 2005; Bertagnini et al., 2008; Francalanci et al., 2008, 2013; Landi et al., 2009; Di Stefano et al., 2020).

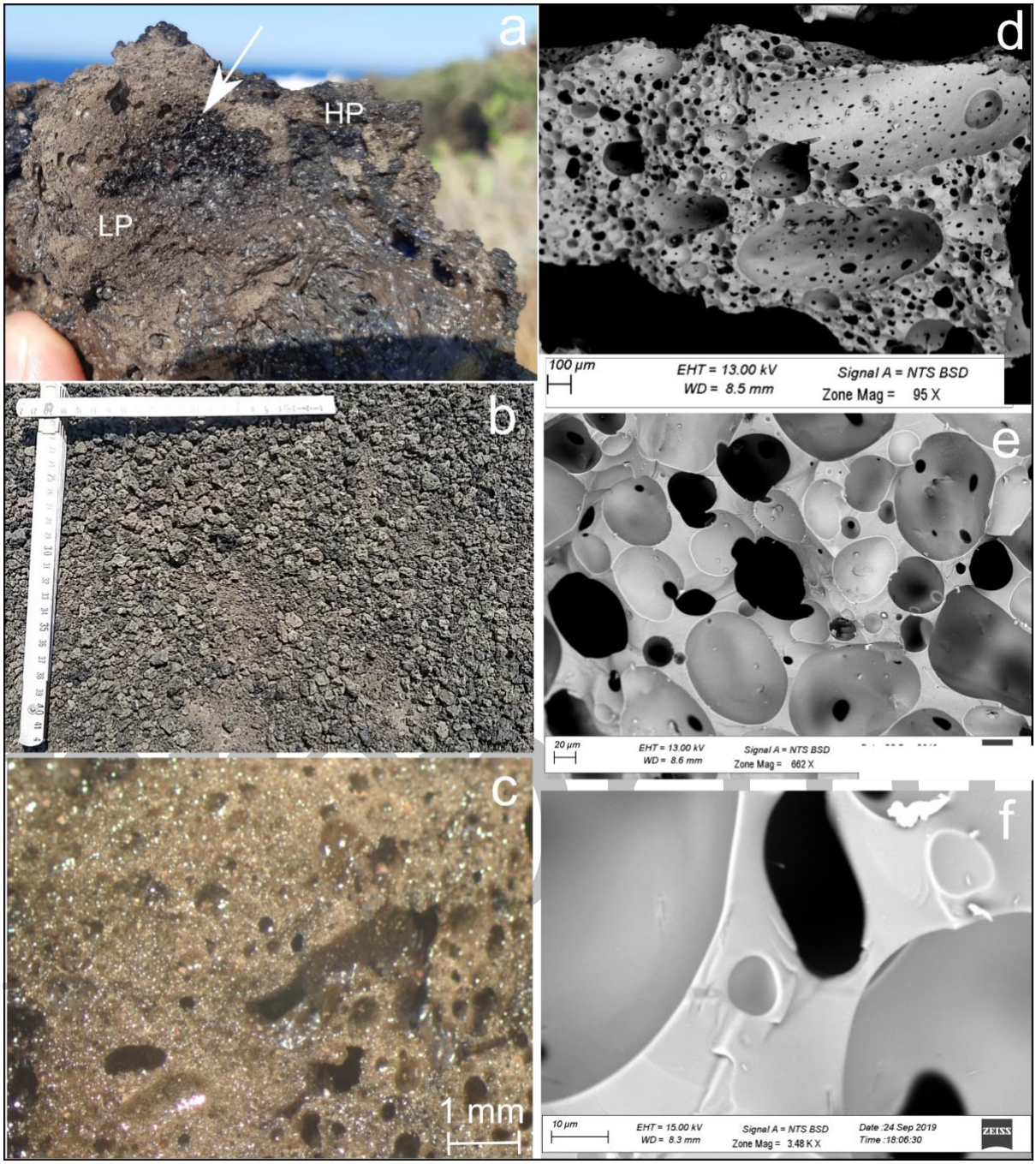

Fig. 2 – a) Ballistic bomb OST1; the bomb shows mingled dark and crystallized HP domains at the outer rim and a frothy, aphyric LP domain in the interior with evidence of post-fragmentation expansion of bubbles at its centre (arrow). b) Plan view of the LP pumice fall deposit at locality GIN1where the total thickness equals the dimension of a single lapilli clast; c) structure of a LP pumice lapillum (GIN1) showing the close packed foam of submillimetric rounded vesicles with dispersed mm-sized more irregular vesicles; d) FE-SEM back-scattered morphological image of a coarse ash particle of LP pumice (GIN8), showing angular shape, evidence of brittle fragmentation, and bimodal distribution of vesicles, with scattered subspherical to elliptical vesicles >2-300 microns in size and abundant spherical vesicles <100 microns in size; e) detail of the spherical small vesicle population at higher magnification (662x); f) high magnification of the smallest vesicle sizes (3480x).

The density of pumice lapilli ranges from 422 to 1494 kg m^{-3}. We find a main population comprising 48 out of 59 measures (81%) in which density ranges between 400 and 1000 kg m^{-3} with a mode at 600 kg m^{-3} (Supplementary material SM2). This corresponds to an 85-64% range of vesicularity (mode 78%) by using the dense rock equivalent density of 2772 ± 12 kg m^{-3} calculated by Andronico et al., (2021) and consistent with previous estimates. Textural analyses have been performed in this density range representative of the LP magmatic foam. Less frequent higher densities, corresponding to lower vesicularities, are not well clustered. At inspection such variability corresponds to clasts with heterogeneous textures due to variable degrees of mingling between HP and LP magma (Viccaro et al., 2021; Visalli et al., 2023) and therefore have not been selected for textural analyses.

SEM binarized images of the analysed samples (Fig. 3; Supplementary material SM3) show rather consistent textural features with some commonalities described below.

The groundmass of the pumice ranges from aphyric to poorly porphyritic (Fig. 2c,d) with rare crystals of pyroxene usually > 0.5 mm in length (Supplementary Material SM3). Microlites are not observed at any magnification.

At low magnifications, the most prominent vesicles are the scattered mm-sized ones, which vary from irregular to subrounded showing smooth internal surfaces (Fig. 3a,e,i, cf. Fig. 2c,d), evidence of coalescence and melt relaxation (Mangan and Cashman 1996).

The sub-millimetric vesicles are substantially different in shape and distribution. Vesicles are mostly spherical to poorly elongated (Fig. 3b,c,f,g,j,k; Fig. 2d,e,f; Elongation/Aspect Ratio R ranging between 1 and 2; Supplementary Material SM4). Their spatial distribution is uneven. More commonly, according to the terminology of Houghton and Wilson (1989), domains are highly vesicular (60-80% vesicularity; *type a*), where vesicles commonly in the range of 100-300 microns appear closely packed and vesicle shapes may become in some cases almost polygonal, similar to reticulite (Fig. 3b,c,k; Mangan and Cashman 1996; cf. texture *type p* in Gurioli et al., 2008); glass walls between vesicles range from few tens to just few microns in thickness (Fig. 3).

Less commonly, domains are moderately to poorly vesicular (vesicularity 20-60%; *type b*) and vesicles are smaller and more widely spaced (Fig.3f,g), with vesicle glass walls that can reach a few hundreds of microns in thickness, but still microlite-free.

Vesicles smaller than ca. 100 microns mostly appear isolated in 2D, whereas larger ones may be isolated or coalesced, at places forming trains of coalesced vesicles (Fig. 3i). Walls of coalesced vesicles smaller than 100 micron show sharp cuspate shapes (Fig. 3b,c), indicating that the melt did not relax between time of coalescence and time of quenching. Larger coalesced vesicles show progressively more evidence of melt relaxation. Walls of mm-sized coalesced vesicles may appear fully relaxed (Fig. 3e).

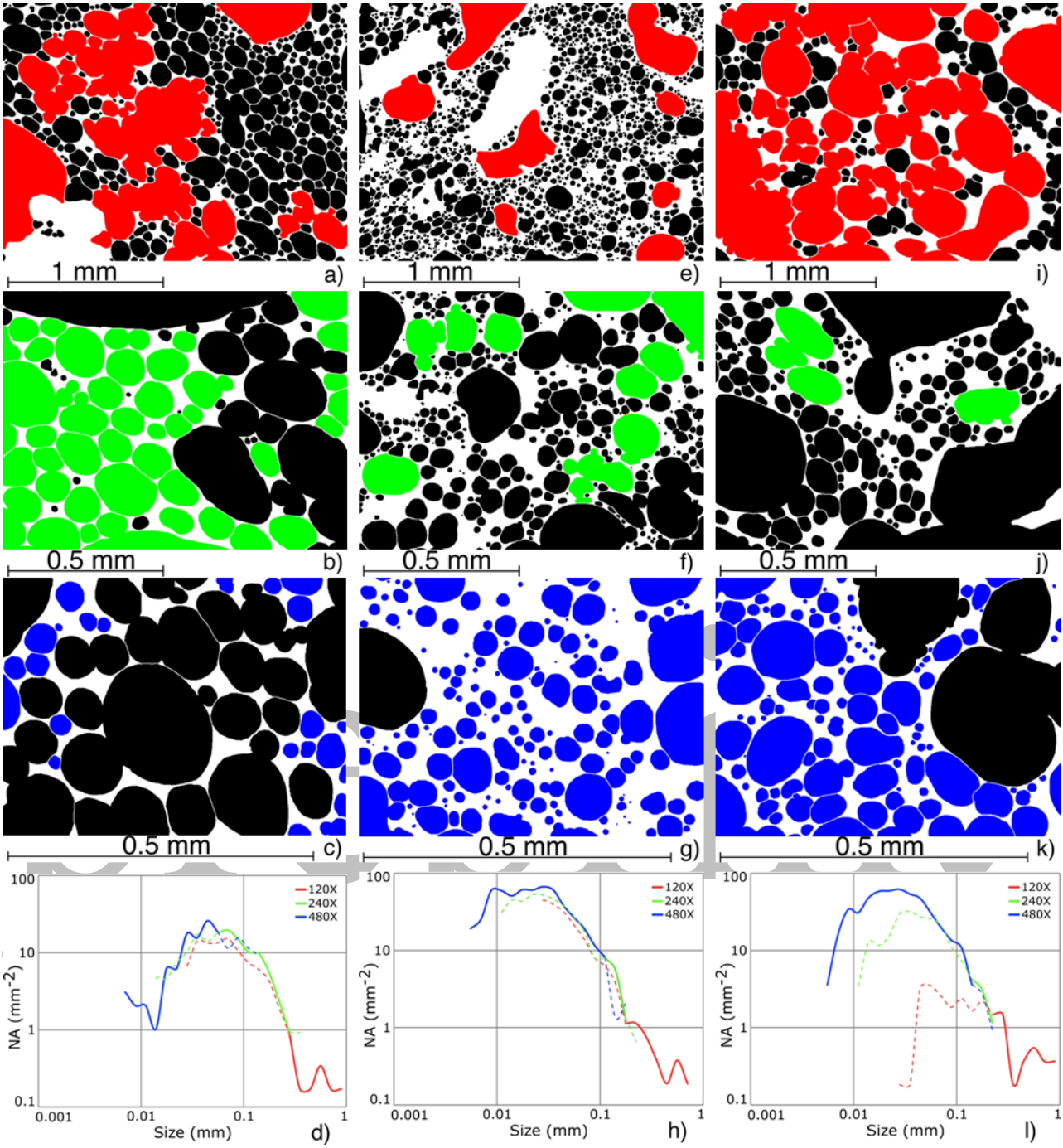

Fig. 3 – Binarized BSE SEM images of selected LP pumice clasts. a-c) sample GIN1-8 at 120x, 240x, 480x; e-g) sample GIN8-4 at 120x, 240x, 480x; i-k) sample GIN8-16 at 120x, 240x, 480x. Vesicles coloured in red, green and blue are those considered for the vesicle size distribution diagrams shown in d), h), l) for GIN1-8, GIN8-4, GIN8-16 respectively (see text for explanation). Unprocessed SEM images are shown in Supplementary Material SM3.

3.2 2D and 3D quantitative measurements of vesicle populations

Textural features derived from 2D images are summarized in Table 2 and shown in Fig. 4 and Supplementary Material SM5. The total porosity ϕ_b ranges from 0.78 to 0.33 (Table 2). These values are consistent with previous estimates (Andronico et al., 2021; Pichavant et al., 2022; Visalli et al., 2023), largely overlapping with those aforementioned from measured bulk densities (Supplementary material SM2) and reflecting the variable distribution of vesicularity inside the clasts.

Vesicle sizes range from 0.004 to 1.742 mm and the Vesicle Number Density (VND) varies between 3.56 x 10^6 and 3.92 x 10^7 cm^{-3} (Table 2), averaging at 1.39 x 10^7 cm^{-3}. These values overlap with the most energetic basaltic explosive products (Sable et al., 2006; Di Traglia et al., 2009; Valdivia et al., 2022) and are consistent with previous estimates for the same products (Andronico et al., 2021; Pichavant et al., 2022).

For samples collected from the lapilli fallout deposit inland (GIN1, GIN6, GIN8) and from the floating pumice rafts (POM), the vesicle volume distributions (VVD) show a main vesicle population forming mostly mesokurtic and dominantly gaussian trends, with a size mode ranging between 0.09 and 0.2 mm, with most samples at 0.1 mm (Fig. 4). To the left of the modes, the distributions of the smaller vesicles show a relatively simple decay, either continuous (e.g. GIN1-4, GIN6c, GIN8-8; Fig. 4) or punctuated by one or two relative peaks (e.g. GIN1-8, GIN1-16, POM; Fig. 4). To the right of the modes, in all samples the larger vesicles show highly variable patterns, resulting in more or less irregular volume distributions and other modes at larger sizes, ranging from 0.5 to 0.9 mm (and larger, but cut in our analysis by the size of the images), out of the mesokurtic range (Fig. 4). Skewness is comprised between 1.05 and 0.63 averaging at 0.78, but clustering at around 1 if the outsized large vesicles are removed from the calculation.

VVD diagrams show that vesicles of the main near-gaussian population, though being the smallest and comprised between 0.08 and 0.3 mm (roughly one standard deviation around the mode), constitute 30-50% of the total vesicularity (Fig. 4).

The VVD from the bomb OST1 is markedly different (Fig. 4), being strongly asymmetric, polymodal and negatively skewed (skewness 0.29).

Cumulative curves of log(VND)-log(size) show well the presence of two vesicle populations that form distinct trends (Fig. 4). The exponent of the smaller vesicle population, which form most of the VND of the sample, is <1, a value consistent with few nucleation events (Bowler

et al., 2001), as described in other studies for the same products (Andronico et al., 2021; Pichavant et al., 2022).

Sample	Area (mm^2)	Porosity	L min (mm)	L max (mm)	VND (cm^{-3})
GIN1-4	13.91	0.48	0.006	0.977	3.56×10^6
GIN1-8	13.91	0.65	0.005	1.742	4.41×10^6
GIN1-16	12.66	0.71	0.005	1.291	1.02×10^7
GIN6	13.91	0.40	0.005	0.659	8.03×10^6
GIN6c	12.91	0.33	0.008	0.651	4.42×10^6
GIN8-4	14.15	0.58	0.004	0.809	3.91×10^7
GIN8-8	13.91	0.68	0.007	0.61	3.19×10^7
GIN8-16	13.91	0.78	0.004	1.256	2.46×10^7
POM	14.41	0.62	0.006	0.885	1.06×10^7
OST1	22.86	0.61	0.006	0.522	6.55×10^6

Table 2 – Summary of textural characteristics of analysed samples (parameters quantified on 2D slides). *L min* and *L max* indicate the diameter of the smallest and the largest vesicle; VND is the vesicle number density. Area is the investigated sample size.

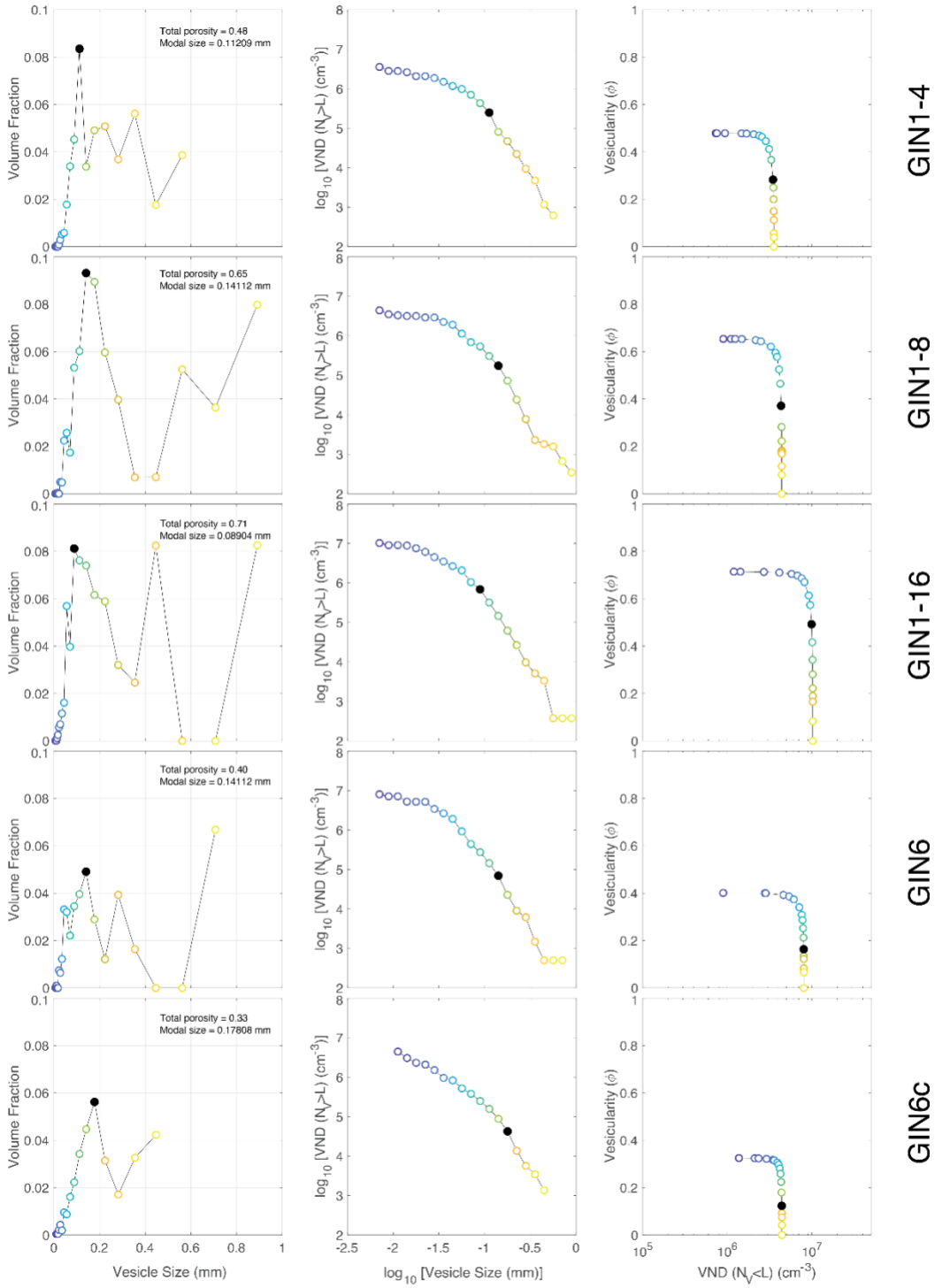
Total porosity = 0.48
Modal size = 0.11209 mm
Total porosity = 0.65
Modal size = 0.14112 mm
Total porosity = 0.71
Modal size = 0.08904 mm
Total porosity = 0.40
Modal size = 0.14112 mm
Total porosity = 0.33
Modal size = 0.17808 mm
Volume Fraction
log10 [VND (N>L) (cm-3)]
Vesicularity (φ)
Vesicle Size (mm)
log10 [Vesicle Size (mm)]
VND (NV<L) (cm-3)
GIN1-4
GIN1-8
GIN1-16
GIN6
GIN6c

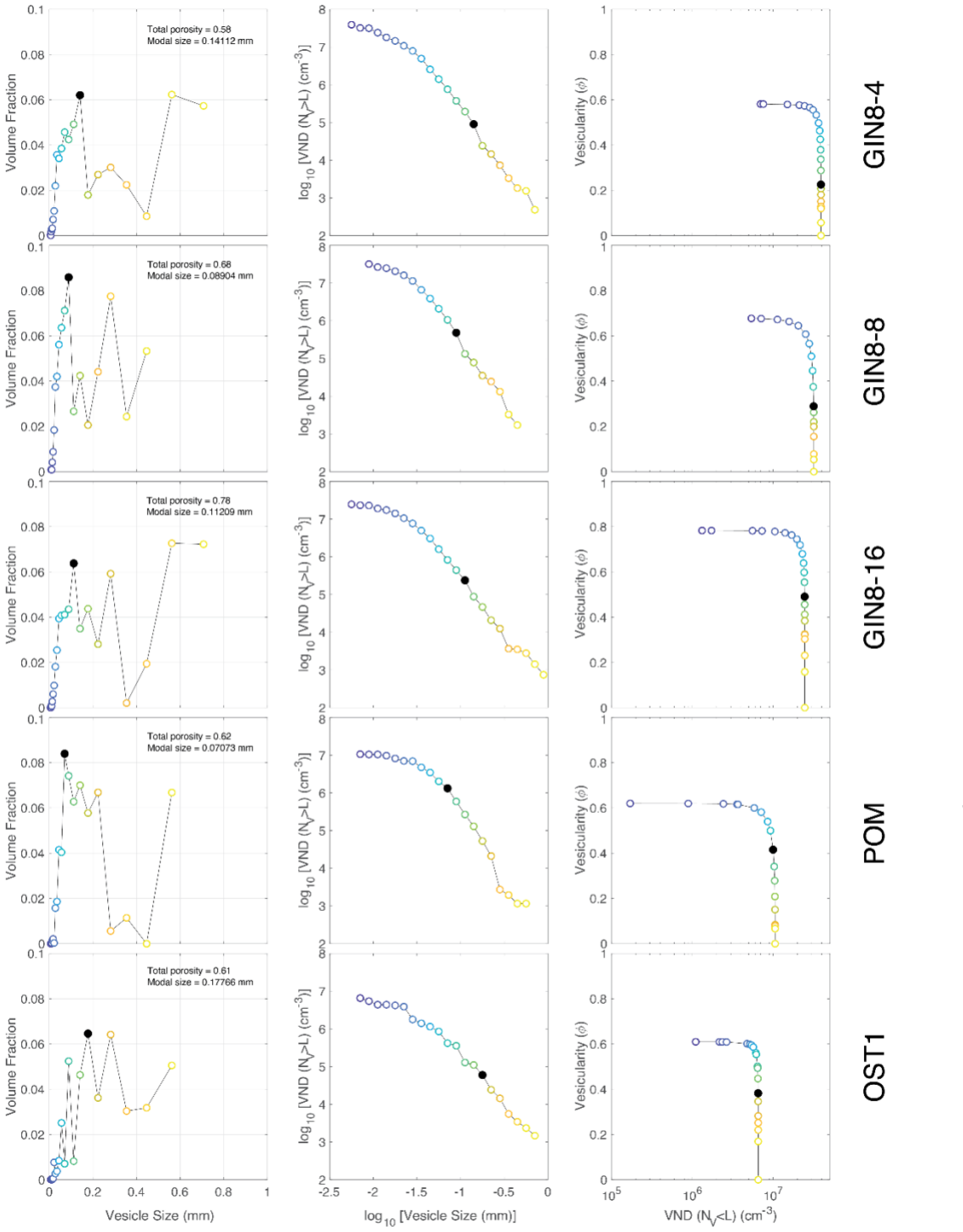

Fig. 4 – Textural characteristics of the analysed samples. For each sample the panel shows the Vesicle Volume Distribution (VVD) histogram (left), the Cumulative Vesicle Size Distribution (CVSD, with the cumulative number density Nv at each vesicle size larger than L) diagram (centre) and the relationship between vesicularity and Cumulative Vesicle Number Density (CVND; with the cumulative number density Nv at each vesicle size smaller than L) (right). The black dots indicate the mode of the main population. The colour code of dots in this

and in Fig. 7 ranges from yellow for the coarsest vesicle size to blue for the smallest and is intended only to help comparing and tracking individual bins across the three diagrams for each sample. The black dot indicates the mode of the small vesicle population.

3D microtomographic imaging of sample GIN3 (Fig. 5) shows the existence of two main populations based on vesicle sphericity (i.e. surface area of a sphere having an equivalent volume of the vesicle/surface area of the vesicle) at the boundary value of 0.87 (Fig. 5e,f; Supplementary material SM6). The spherical porosity (>0.87 sphericity) dominates the vesicle smaller than 150 microns (Fig. 5g).

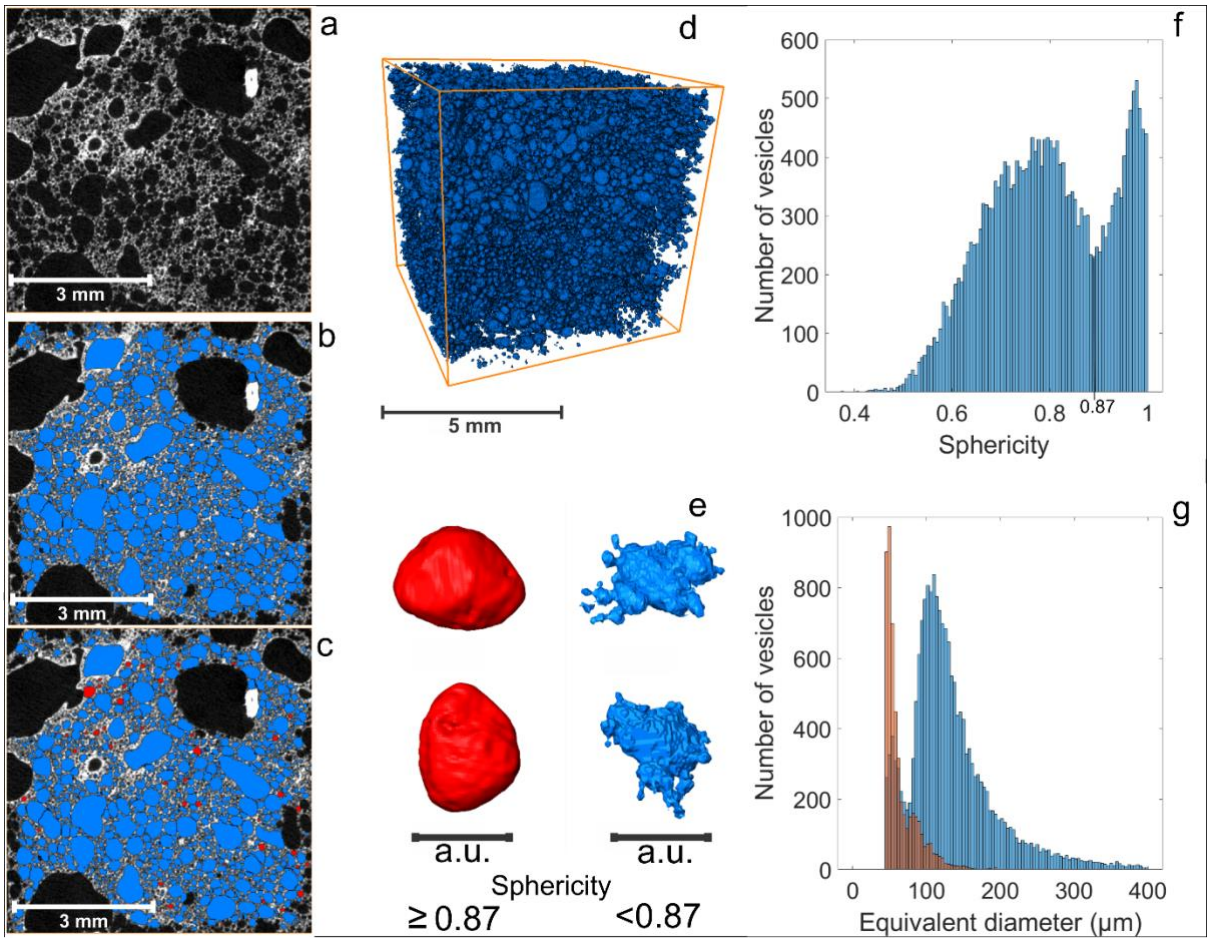

Fig. 5 – 3D microtomography of sample GIN3. Processing stages: (a) filtering to eliminate noise, (b) segmentation of the porous medium, (c) separation of two porosity populations; in red pores with sphericity greater than or equal to 0.87 and in blue lower than 0.87, (d) three-dimensional view of the sample, (e) shapes of vesicles with sphericity ≥0.87 in red, and ≤0.87 in blue. f) Distribution of pore sphericity showing the existence of two populations separated at 0.87. g) Equivalent diameter of pores: in red pores with sphericity ≥0.87, in blue ≤0.87.

A total porosity for sample GIN3 is estimated at about 0.58, with a comparable effective porosity of 0.56, suggesting that almost all vesicles are connected. However, applying an anisotropic diffusion filtering (Perona and Malik 1990; Supplementary material SM5) it is possible to enhance the original spherical shape of the vesicles for the coalesced porosity (cf. Toramaru 1990), which result in very irregular shapes (Fig. 5e), further highlighting the lack of significant melt relaxation after coalescence, as also well evident in the 2D images (Fig. 3). In addition, it should be noted that the resolution of the microtomographic images does not accurately resolve features smaller than 10 microns. Consequently, the coalesced porosity may actually include isolated spherical vesicles separated by septa smaller than the image resolution (cf. Fig. 3).

4 Discussion

The use of the term "paroxysm" to identify an eruption style has been already questioned (e.g. Cashman and Scheu 2015). More recently Giordano and De Astis (2021) discussed how all phenomenological aspects of the 2019 "paroxysms" at Stromboli and their deposits match those typical of the Vulcanian eruption style. A similar consideration was made by Calvari et al. (2006) for the 2003 paroxysmal event. Notably the 2019 proximal deposits form a thin blanket of ballistic lithic fragments and disrupted HP magma spatter related to the vent blasting and conduit clearing phase (seconds) that preceded the short-lived plume phase (minutes) dominated by the LP pumice. However, the key genetic feature of Vulcanian eruptions, as currently defined, is the sudden failure of a shallow cap (a rigid magma plug/dome or just a close conduit) under the action of pressurizing magma at the base of the plug or by gravitational instability. These conditions are similar to those shown by phreatic eruptions, where just gas is involved and an impermeable cap under which pressure can be accumulated (Montanaro et al. 2022; Stix et al. 2025). This failure generates a downward-propagating decompression wave that triggers vesiculation and fragmentation of the magma residing in the conduit at shallow depth, once the plug is blasted away (Clarke et al., 2015). This conceptual model can be hardly applied to open conduit basaltic volcanoes where magma viscosity is too low to allow significant overpressurization of the magma in the conduit, even in the presence at its top of degassed and crystallized magma, which may form the so-called "weak or soft plug" (Del Bello et al., 2015; Oppenheimer et al., 2020; Caracciolo et al., 2021). For these reasons, despite the obvious similarities of the "paroxysms" at Stromboli with Vulcanian eruptions, there has been

little effort in investigating possible alternatives to the "standard model" that explains "paroxysms" as caused by fast rise from depths of 7-10 km of a volatile-rich small batch of magma that expands by volatile exsolution as a closed system, perches with its momentum the magma filling the conduit, and eventually triggers the explosive eruption (e.g. Bertagnini et al., 2011; Métrich et al., 2010, 2021; Petrone et al., 2022; Pichavant et al., 2022).

We discuss below the vesicularity of the fresh magma juveniles (i.e. the LP golden pumice) erupted on July 3rd, 2019, at Stromboli, and propose an alternative model for the trigger of these explosive events. We argue that eruptions such as that of the July 3rd, 2019, may be better explained by a sudden decompression event affecting the LP magma accumulated at 2-4 km depth in the months-days-hours prior to the eruption. The trigger for this sudden decompression is, in our interpretation, the failure of the shallow (< 2km) HP magma weak plug pressurized by the rise of a large gas slug from depth, which is a mechanism very similar to what is envisaged for Vulcanian eruptions.

4.1 Textural evidence for very short timescales of bubble nucleation, growth, coalescence, fragmentation and quenching

Textural characteristics record the history of pyroclasts, from vesiculation, bubble nucleation, growth and coalescence across fragmentation, and up to quenching when crossing the glass transition interval (e.g. Mangan and Cashman 1996, Toramaru 2006; Shea et al., 2010). The July 3rd, 2019, plume fallout deposit, similar to all other "paroxysms" at Stromboli, is dominated by LP pumice with low density comprised between 400 and 1000 kg m^{-3} and bulk vesicularity in the range 85-64%. This material had erupted sequentially after the full evacuation of the HP magma filling the shallowest part of the conduit (Fig. 1; Giordano and De Astis, 2021).

The VVD analysis shows that the vesicularity of the LP pumice lapilli (GIN1, GIN6, GIN8, POM) is dominated by a fine vesicle population with a near-gaussian mesokurtic distribution, with a mode comprised between 0.09 and 0.2 mm. Vesicles larger than 0.3 mm form a distinct population (Fig. 4) dominated by processes of coalescence (Figs 2 and 3) which result in modes at larger sizes (Fig. 4; Shea et al., 2010). The coalesced population becomes dominant in the analyzed bomb samples (OST1), where the shift to polymodal and negatively skewed coarse vesicle population reflects post-fragmentation coalescence to the expenses of the smaller sizes

(Fig. 4; Mangan and Cashman 1996; Shea et al., 2010). We conclude that, differently from larger bombs, the texture of the LP pumice lapilli has not been significantly affected by post-fragmentation processes and is therefore representative of the state of the magma at fragmentation.

The fine vesicle population constitutes up to 50% of the vesicularity and the bulk of the VND, ranging between 10^6 and 10^7 cm^{-3} and exceeding the VNDs determined for other paroxysms at Stromboli (cf. Pichavant et al., 2022). Cumulative log(VVD)-log(size) curves show a mixed exponential and power-law trend with a low exponent, which, together with all other described textural parameters, are indicative of rapid bubble nucleation and growth under significant disequilibrium conditions associated with few nucleation events (Mangan and Cashman, 1996; Blower et al., 2001; Shea et al., 2010).

The fine vesicle population is essentially undeformed, spherical to subspherical in shape (Figs 2d,e,f and 3). The coarse vesicle population is less spherical (Fig. 2c,d and 3a,e,i), but elongations are not preferential, with no common evidence for simple or pure shear-induced deformation.

Our results appear qualitatively and quantitatively consistent with textural data presented in the literature. However, while data are consistent, in contrast with previous interpretations (cf. Andronico et al., 2021; Pichavant et al., 2022), we cannot reconcile them with a prolonged decompression history of the LP magma along a several km-long conduit at relatively slow ascent rates of 1-2 m s^{-1} as modeled by Pichavant et al. (2022). Rather, we interpret our quantitative textural data as reflecting a very fast and short-lived magma decompression event affecting the LP magma, which better explains the observed (i) high VND and (ii) the few nucleation events.

The coupled high vesicularity and absence of microlites in the groundmass glass is additional evidence for very fast degassing of the low viscous Stromboli melt, determining a severely undercooled melt far from its physicochemical equilibrium that, in turn, did not reach thermodynamic conditions for crystal nucleation and growth within the eruption timescale (Scarani et al.,, 2022; Di Fiore et al., 2024).

A short-lived decompression event is consistent with very short decompression space, therefore with a shallow decompression.

Very short quenching timescales of lapilli after fragmentation are constrained by the ubiquitous cuspate shapes of the throat openings of coalesced vesicles < 0.5 mm (Fig. 3). As melt had no time to relax after coalescence, the timescale of quenching must have been faster than the bubble relaxation time. It is important to notice that while coalescence is almost totally unrelaxed within the high VND small vesicle population (Figs 2c, 3 and 5E), the low VND large vesicles show smooth surfaces (Figs 2c,d and 3d,g) suggesting different timescales for their coalescence. This evidence may suggest that the low VND, large vesicle population may represent "phenobubbles" (Toramaru, 2014), i.e. bubbles already present in the LP magma before decompression and the final fast uprise event.

Pumice lapilli floating in the sea for weeks confirm the unique structure of LP vesicularity, which, even if porosity is dominantly interconnected, did not allow water to penetrate the clasts. Mitchell et al (2021) suggest for the floating felsic pumice generated by the 2012 submarine Havre eruption, that the micron-size dimension of coalesced vesicle throat openings may explain their floating behaviour, which seems applicable also to the Stromboli LP pumice.

All the described textural features for the LP pumice lapilli strikingly contrast with those of pyroclasts of fire fountains and violent Strombolian products, in which the geophysically detectable fast rise of fresh volatile-rich basaltic magma from depth over timescales of hours (e.g. Viccaro et al., 2014; Spampinato et al., 2015; Cardone et al., 2024) results in mixed deposits of sideromelane and tachylite (e.g. Taddeucci et al., 2004; Marsh et al., 2024). In such conditions, erupted products are dominated by scoria with polymodal and usually skewed VVDs as a result of multiple events of nucleation, growth and coalescence during magma rise through the conduit (Mangan and Cashman 1996), and common if not ubiquitous presence of microlites in the groundmass (e.g. Johnson et al., 2008; Polacci et al., 2008; Holt et al., 2019; Bonechi et al., 2024; Marsh et al., 2024).

We conclude that LP pumice texture cannot be reconciled with the "standard model" of a small batch of magma rising across a conduit several kilometers long. By contrast we interpret this texture as reflecting a sudden decompression event affecting the LP magma already residing in the conduit at relatively shallow depths (>2 km; cf. Viccaro et al., 2021; Mattia et al., 2021; Visalli et al., 2023), causing its sudden vesiculation, fragmentation, eruption and quenching in very rapid succession. This scenario is that of a Vulcanian eruption and in the next section we explore possible trigger mechanisms that could apply to a basaltic open conduit volcano like Stromboli.

4.2 Basaltic Vulcanian eruption style: A gas slug trigger for the sudden pressurization and failure of the shallow HP magma weak plug, top-down decompression of the LP magma, and distinction between long-term and short-term processes and monitored signals.

Any alternative to the "standard model" for Stromboli "paroxysms" must consider the wealth of existing data and consolidated knowledge about processes and timescales that precede such explosive eruptions.

Petrology, mineral chemistry, and gas geochemistry data converge in defining timescales of months to hours for the recharge of the deep part of the plumbing system filled with LP magma, which extends in depth between 7-10 km and 2-4 km from the summit (Fig. 6a; Métrich et al., 2010, 2021; Petrone et al., 2022; Pichavant et al., 2022; Landi et al., 2022; Caricchi et al., 2024; Insiga et al., 2025). These timescales characterize the "long-term" build-up phase that may precede "paroxysms" and are accompanied by an increase in CO_2 flux at the vent, which tracks the progressive recharge of LP magma from deep (7-10 km) to shallower levels (2-4 km)(Aiuppa et al., 2021; Caricchi et al., 2024; Stix et al., 2025). Geophysical signals (seismicity and deformation) during this same long-term timescale have been extensively investigated and do not show any clear or significant variation (Di Lieto et al., 2020), except for the increase in size of the shallow very long period seismicity in the month preceding the July 3rd eruption (Giudicepietro et al., 2020, 2022; Di Traglia et al., 2021; Mattia et al., 2021). This suggests that processes of deep magma recharge are largely accommodated within the low viscous LP magma plumbing system and have gone undetected (Fig. 6a), at least by the current configuration of the monitoring network. Only at about 2 hours before the event, Ground Based InSar (GBInSar) data showed the beginning of a mild inflation of the subaerial edifice, which became noticeable in terms of rate and amplitude only few minutes before the eruption in agreement with other ground deformation data (see below; Di Traglia et al., 2021). Therefore, none of the long-term (months to hours) geochemical and geophysical signals is considered an unequivocal precursor of the July 3rd, 2019, eruption and even less of its impulsive, energetic and unexpected Vulcanian style, as their fluctuations over time and absolute values do not necessarily anticipate a paroxysmal eruption, such it happened in 2014 when similar long-term monitoring patterns resulted in just effusive activity (Rizzo et al., 2015; Di Traglia et al., 2018).

So far the only monitored signal unequivocally identified as precursor is the rate and amplitude of the volcano summit inflation that preceded by minutes the eruption, measured by tiltmeters, strainmeters and GBInSar, and which point to very shallow sources of pressurization, located

within the subaerial part of the volcanic edifice, at few hundreds of meters below the crater terrace (Figs 1b and 6a; Di Lieto et al., 2020; Giudicepietro et al., 2020; Di Traglia et al., 2021; Mattia et al., 2021; Ripepe et al., 2021; Viccaro et al., 2021).

It is therefore essential to highlight that there is a clear distinction between the long-term processes and signals that track the evolution in time of the deep plumbing system that may or may not lead to paroxysmal eruptions, from the short-term processes and signals that are instead unequivocal precursors of the specific eruption style exhibited by the so-called Stromboli paroxysms.

Therefore, from here onwards, we focus on the mechanisms for the short-term (minutes) pressurization and triggering of the eruption. The source depth of the pressurization that immediately preceded the July 3rd, 2019, eruption at Stromboli has been inverted from ground deformation data at depths of 240-380 m below the vent (350-470 m a.s.l.) by Ripepe et al., (2021) and at ca. 650 m below the vent (100 m a.s.l.) by Viccaro et al. (2021) and Mattia et al. (2021). These depths correspond to the VLP earthquake localizations and the inferred GBInSAR pressure source at 150-550 m depth below the vent (200-600 m a.s.l.) in the period May-August 2019 (Giudicepietro et al., 2020, 2022) (Fig. 6a). Di Lieto et al. (2020) suggested that the deformation initiated from a slightly deeper source at ca. 1.4 km depth and then migrated upward, possibly as the upward migration of a large gas slug (Fig. 6a).

Considering that: i) the viscous HP magma fills at least the upper 2 km of the Stromboli conduit (Pichavant et al., 2022; Patané et al., 2007; Métrich et al., 2010) (Fig. 6a); ii) the only significant event that may have partially evacuated the HP magma from the conduit before the eruption was a small intra-crateric lava overflow that preceded the July 3rd paroxysm by 2.5 minutes (Giudicepietro et al., 2020), which may have removed HP magma from just a few tens of meters of the conduit at most; there is no doubt that the pressurization and explosion of the July 3rd, 2019 occurred well within the shallow conduit filled with HP magma (Fig. 6a; cf. Viccaro et al., 2021; Ripepe et al., 2021), as clearly demonstrated by the early erupted HP spatter cover that blankets the summit area (Fig. 1).

Ripepe et al. (2021) demonstrated that the tilt associated with explosions of any size at Stromboli, from ordinary Strombolian to large-scale paroxysms, shows the same shape when normalized. This indicates a relatively invariant source and process of pressurization at shallow depths within the HP column where the difference in amplitude relates to the size of the

pressure source and the pressurization rate (Ripepe et al., 2021). It is widely accepted that pressurization during ordinary Strombolian activity, such as that prevailing before the July 3rd, 2019, eruption, is associated with the rise of gas slugs (e.g. James et al., 2008; Gurioli et al., 2014; Del Bello et al 2015 and references therein). In these conditions, excess pressurization within the shallow HP magma can be achieved only if its permeability threshold is suddenly exceeded. We envisage that the arrival of a large gas slug can suddenly increase the influx of gas that accumulates at the base and forced throughout the HP magma (Fig. 6a). This process pressurizes the shallow HP magma as the gas cannot fully percolate through its permeable network (e.g. Allard 2010; Mattia et al., 2021; Insiga et al., 2025), and its upward expansion results in the HP expanding and deforming the summit edifice. Giudicepietro et al. (2022) noticed a progressive increase in the number of gas-driven explosions in the month preceding the July 3rd eruption and suggested a possible progressive densification of the HP magma filling the conduit, a condition which may lead to a reduction in its permeability.

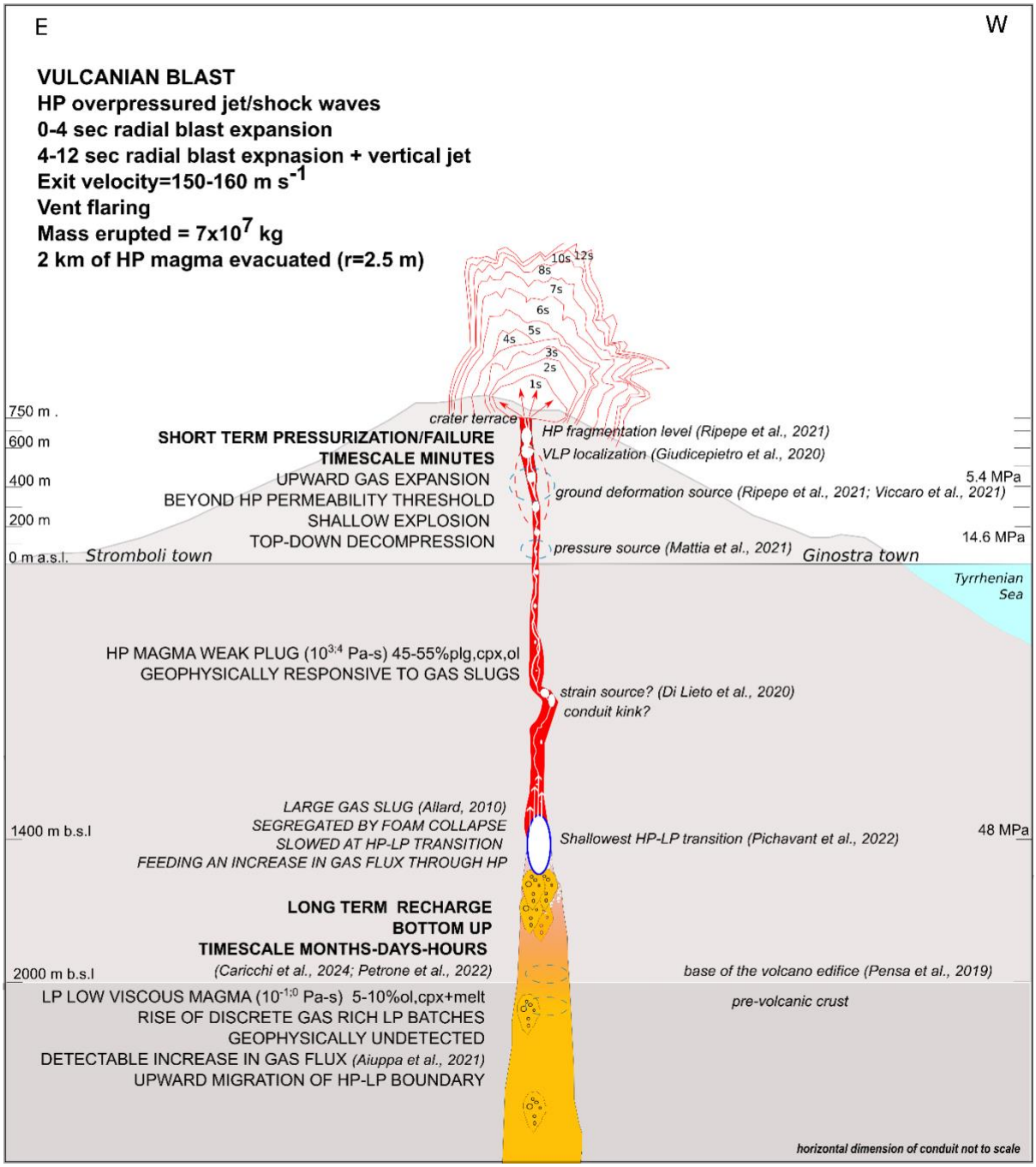

Fig. 6a - Conceptual model for the origin of the July 3rd, 2019, basaltic Vulcanian eruption at the open conduit Stromboli volcano. a) The panel synthetizes the bottom-up long-term (months to days/hours) recharge processes within the deep LP magma (in yellow) recorded by mineral chemistry and gas geochemistry, and the short-term (minutes) failure of the shallow HP-filled conduit (in red) as a consequence of the segregation and upward migration of a large gas slug that increases the gas flux through the HP-filled conduit beyond its percolation threshold; the consequent failure of the very shallow conduit triggers the Vulcanian blast, the flaring of the vent and the radially-expanding jet (first 12 seconds of the eruption; line-drawing from Giordano and De Astis, 2021) and a top-down decompression able to recall the remaining HP and the LP magma present in the conduit depicted in (b).

We therefore envisage the short-term, sudden (minutes) pressurization of the shallow HP magmatic column, as induced by the overcoming of its permeability threshold due to the arrival and expansion of a large gas convoy (Fig. 6a; cf. Allard, 2010; Viccaro et al., 2021). This mechanism accounts for calculations in Ripepe et al. (2021), indicating that the expansion rate of the HP magma reached conditions for fragmentation at depths comprised from few tens of meters down to 150 m, consistent with the observed shallow explosion dynamics and vent clearing processes (Figs 1 and 6a).

Allard (2010) proposed that gas slug triggering paroxysms form by a foam collapse process (Parfitt 2004), where the thickening of a bubble-rich layer (Woods and Cardoso 1997) may eventually lead to critical conditions when the gas suddenly separates from the bubbly magma, forming a gas slug readily able to rise separately from the melt (Jaupart and Vergniolle 1989). The dimensions of the gas slug depend on the thickness of the collapsing foam, which is likely larger during waxing degassing phases, as observed before in the months preceding paroxysms (Aiuppa et al., 2021; Caricchi et al., 2024; cf. also Insiga et al., 2025 for similar conditions suggested for major explosions). This seems confirmed by the progressive increase in VLP size observed in the month prior to the eruption, located at invariant shallow depths (Figs 1 and 6a; Giudicepietro et al., 2020), which may suggest that the dimension of the gas slugs percolated throughout the HP upper conduit increased over time in size and frequency (see also Giudicepietro et al. 2022), in agreement with the model of deep recharge proposed by Caricchi et al. (2024).

While timescales and depths of the foam growth, collapse and slug formation are difficult to reconstruct from the geophysical and geochemical long-term record, we concur with Allard (2010) that the segregation of a large gas slug and its upward migration are the likely conditions that can force an increase in gas flux through the HP magma filling the upper conduit and its progressive and upward pressurization due to gas expansion (Fig. 6a; cf. Ripepe et al., 2021). The pre-eruptive pressurization phase corresponds to the last 10 minutes of strong inflation of the volcano summit before the explosion, with pressure sources located in the shallowest 650 m of conduit, i.e. between sea level and the vent (Figs 1b and 6a). The increase in gas flux above the HP permeability threshold and consequent pressurization of the HP magma may have forced first the HP magma upward (i.e. the small lava overflow issued at about 2.5 minutes before the explosion; Giudicepietro et al., 2020) and then to explosion few tens to 150 m below

the vent, where the lateral confining pressure of the volcano edifice becomes too small (Ripepe et al., 2021; Figs 1b and 6a). This explains the vent flaring by 70 m (Civico et al., 2021), the launching of ballistic blocks, the occurrence of shock waves and the initial overpressurized radial expansion of the blast (Fig. 1a,b; Fig. 6a). The very shallow explosion and the removal of the HP magma from the top of the magmatic column is interpreted as the trigger for the subsequent very rapid top-down decompression and evacuation of the rest of the HP magma from the conduit. Decompression fast propagated downward into the conduit as a rarefaction wave (Turcotte et al., 1990; Woods, 1995), allowing the gas rich top of the LP magma filling the conduit below 2 km depth to suddenly expand. The sudden foaming of the LP magma resulted in its very fast ascent and fragmentation which then fed the buoyant plume phase (Figs 1d and 6b). The sequential top-down evacuation of, first, the shallow HP magma, followed by the LP magma, is recorded by the zoned deposit stratigraphy: the early erupted HP spatters form the base of the deposit succession and occur dominantly in the summit area where the initial blast was ballistically emplaced (Fig. 1a,b,c), whereas the later erupted LP pumice is present at the top and widely transported by the buoyant 8.4 km high plume (Fig. 1c,d; Giordano and De Astis 2021; Andronico et al 2021).

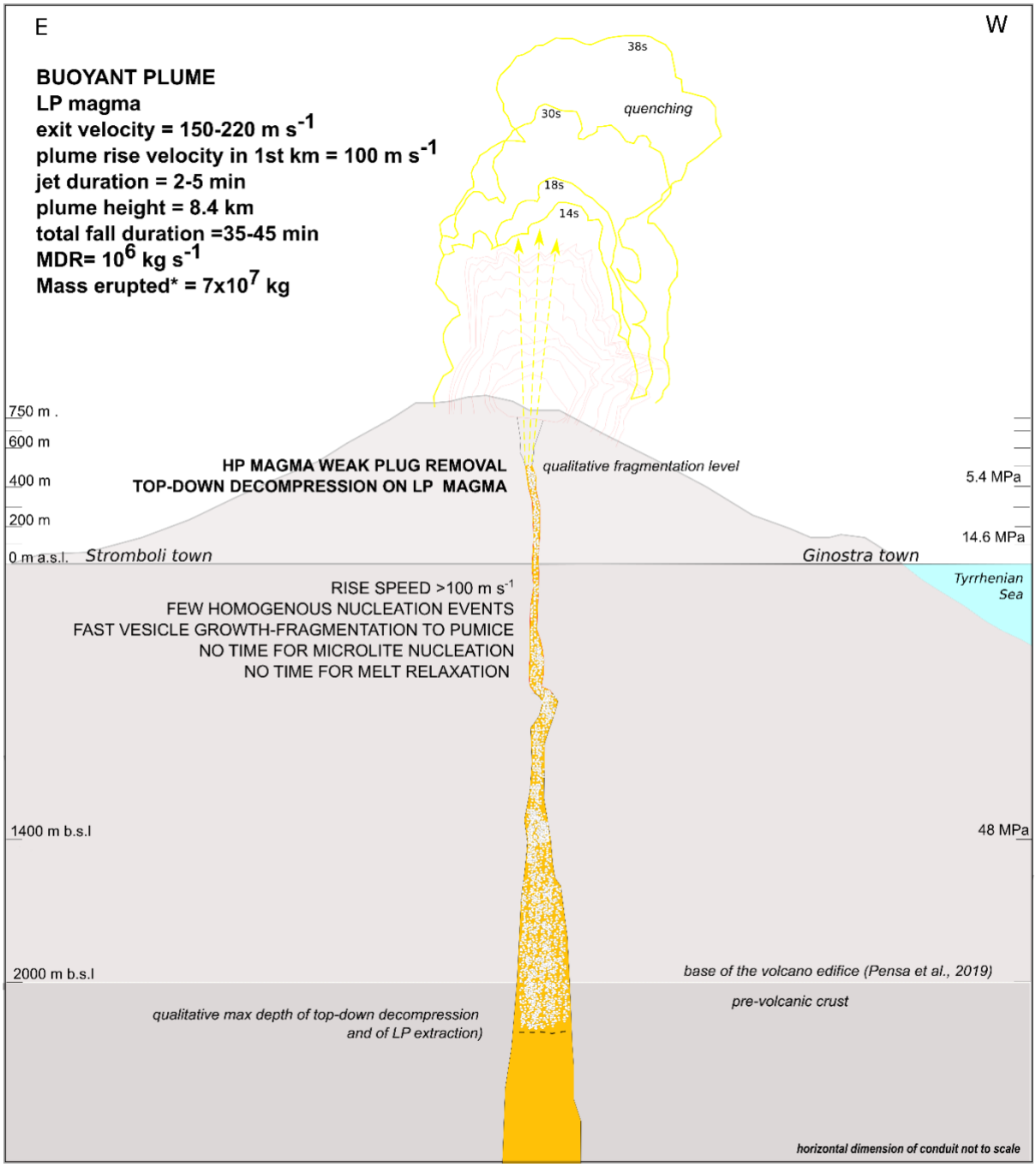

Fig. 6b - Conceptual model for the origin of the July 3rd, 2019, basaltic Vulcanian eruption at the open conduit Stromboli volcano. b) Once the HP magma is fully removed from the shallow conduit (panel a), the downward propagation of a rarefaction wave allows the fast vesiculation, expansion and the very fast ascent of the LP magma at near-closed degassing conditions, which explains the formation of microlite-free LP pumice foam and its brittle fragmentation despite the very low viscosity. This phase of the eruption lasted 2-5 minutes feeding a convective plume (line-drawing up to 38 seconds from Giordano and De Astis 2021) and ended once the mass of LP magma erupted equilibrated the mass of HP magma removed re-filling the shallow conduit.

In order to physically constrain our proposed conceptual model, it is essential to verify whether it can explain the observational phenomena at surface and the textural data.

The initial blast on July 3rd, 2019, lasted 4 seconds as a pure radial expansion of the pyroclastic jet (Figs 1a,b and 6a), then accompanied, until 12 seconds, by the simultaneous development of a vertical component (Fig. 6a; Giordano and De Astis, 2021). We interpret the first 4 seconds as those related to the very shallow explosion of the HP magma, followed up to 12 seconds by the drainage of the remaining pressurized HP magma from the conduit (Fig. 6a). During this early phase a volume of ~7 x 10^4 m^3, corresponding to a mass of ~9 x 10^7 kg of HP spatter (considering a spatter density of 1350 kg m^{-3}; Giordano and De Astis, 2021) was ballistically deposited at the summit (Fig. 1c; Table 1; Giordano and De Astis, 2021). Assuming a conduit radius of 2.5 m (e.g. Misiti et al., 2003; Del Bello et al., 2015), and considering a density of the HP magma residing in the shallow conduit at 2300-2500 kg m^{-3}, based on a permeable bubble network of 10-20% volume to allow continuous degassing (cf. Rust and Cashman 2004), we estimate that ~ 2 km of the HP conduit were drained (Fig. 6a,b). Knowing depth and timing of evacuation, the resulting ascent velocity of the HP magma is estimated to be ~ 160-170 m s^{-1}, driven by gas expansion (Supplementary Material SM7). These values align well with exit velocity derived from the ballistic blocks at ~150-160 m s^{-1} (Giordano and De Astis 2021), and at 200-250 m s^{-1} from video frames analyses (Andronico et al., 2021), which account for gas expansion after fragmentation. Notably, the observations on the initial blast and the related calculated values are very similar to those made for the 1997 Vulcanian eruptions at Montserrat (Fromenti et al., 2003).

After 12 seconds since eruption onset, the plume transitioned from the initial radially expanding, overpressurized blast (Fig. 6a) to a vertically directed plume that transported the LP (and to a minor extent LP-HP mingled) pumice lapilli fallout onto the island and offshore (Figs 1d, 2 and 6b). To estimate the ascent rate of the LP magma, we use the mass eruption rate of 1.1 x 10^6 kg s^{-1} (equivalent to a volumetric eruption rate of 385 m^3 s^{-1}) derived from plume height reported by Giordano and De Astis (2021). Using the same conduit radius of 2.5 m and a density of the rising LP magma ranging from its dense value of 2776 kg m^{-3} (Andronico et al., 2021) to 1000 kg m^{-3} (representing the foam just below fragmentation level), the ascent velocity is estimated to range between 20 and 56 m s^{-1} (Supplementary Material SM7).

The rapid LP ascent and the short-lived mechanism are consistent with the absence of microlites, and the relatively small volume erupted (Giordano and De Astis 2021, Andronico

et al., 2021) compared to fire fountains and violent Strombolian eruptions (e.g. Calvari et al., 2018).

Interestingly, there is a striking agreement (within uncertainties) between independent estimates of (i) the HP spatter volume linked to shallow conduit evacuation by Giordano and De Astis (2021) and (ii) the LP fallout volume by Andronico et al., (2021) (Table 1; Fig. 6a,b). This may suggest that the eruption of LP magma ceased once the conduit was replenished and pre-eruptive near-magmastatic conditions restored, supporting a top-down trigger mechanism and a passive role of the LP magma that had no extra overpressure to further maintain the eruption.

Decompression rates of the LP magma from VND data, can be calculated following Eq. 1 (Toramaru, 2006; Shea 2017):

$$VND = 34X_0\left(\frac{16\pi\sigma^3}{3kT{P_0}^2}\right)^{-2}\left(\frac{\Omega_M P_0}{kT}\right)^{-\frac{1}{4}}\left(\frac{kTX_0D{P_0}^2}{4\sigma^2\left|\frac{dP}{dt}\right|}\right)^{-\frac{3}{2}} \quad \text{(Eq. 1)}$$

where X_0 is the water content at saturation pressure, dP/dt is the decompression rate (MPa s^{-1}), k is the Boltzman constant (m^2 kg s^{-2} K^{-1}), Ω_M is the volume of water within the melt assumed as equal to 2.6 x 10^{-29} m^3, P_0 is the saturation pressure, T is the absolute temperature (°K), σ is the surface tension (N m^{-1}) and D is water diffusivity (m^2 s^{-1}; Zhang and Ni, 2010).

Equation 1 requires the definition of the initial LP magma H_2O contents and surface tension. The initial water contents have been determined according to the water solubility profile for the average chemical composition of the LP magma (Métrich et al., 2021), taking into consideration the persistent flushing of CO_2 through the magma column as described in Caricchi et al. (2024), using MagmaSat (Ghiorso and Gualda, 2015). We set three scenarios for each pressure, with the excess fraction XH_2O in the fluid phase ranging between 0.75 and 0.25, the rest being CO_2. The pressure range for the LP magma mobilized during the eruption has been calculated to test the proposed conceptual model, with the pre-eruptive configuration described in Fig. 6a, where (i) the density of the vesicular HP magma is 2500 kg m^{-3} as defined above, (ii) that of the dense LP magma is 2776 kg m^{-3} (Andronico et al., 2021), (iii) the erupted LP magma was sitting between 2 and 4 km, that is our selected scenario. For these conditions, the pre-eruptive LP magma pressures were approximately between 50 and 100 MPa. Initial

H_2O contents at saturation range from a minimum of 0.86 wt% at 50 MPa at a fraction of H_2O in the excess fluid of 0.25, to a maximum of 2.62 wt% at 100 MPa at a fraction of H_2O in the excess fluid of 0.75 (Supplementary material SM8). By taking the intermediate values at a fraction of H_2O in the excess fluid of 0.50, H_2O contents range between 1.33 and 1.95 wt% which we adopt for our calculations. Further, according to Di Piazza et al., (2019) we consider the amount of H_2O that was effectively present during the nucleation and growth of the distinct small sized vesicle population with mode comprised between 0.09 and 0.2 mm recognized in our samples (Fig. 7). This population experienced the last phase of decompression during the eruption. The effective water contents range between 1.07 and 0.64 wt% (Table 3). The effective VND values related to the modes range between 3.48 x 10^6 and 3.91 x 10^7 cm^{-3} (Table 3).

Sample	Modal L	VND_{eff}	H_2O_i (wt%) =1.33				H_2O_i (wt%) =1.95			
			H_2O_{eff}	P_{eff}	h_{eff}	dP/dt	H_2O_{eff}	P_{eff}	h_{eff}	dP/dt
	(mm)	(cm^{-3})	(wt%)	(MPa)	(km)	MPa s_{-1}	(wt%)	(MPa)	(km)	MPa s_{-1}
GIN1-4	0.112	3.48×10^6	0.85	21.23	0.87	0.43	1.13	36.04	1.47	0.48
GIN1-8	0.141	4.34×10^6	0.76	16.97	0.69	0.47	0.99	28.46	1.16	0.52
GIN1-16	0.089	9.92×10^6	0.64	12.46	0.51	0.77	0.83	20.22	0.82	0.85
GIN6	0.141	8.01×10^6	1	29.16	1.19	0.79	1.37	51.92	2.12	0.89
GIN6C	0.178	4.41×10^6	1.07	32.41	1.32	0.55	1.47	59.57	2.43	0.61
GIN8-4	0.141	3.91×10^7	0.92	24.76	1.01	2.18	1.24	42.52	1.73	2.49
GIN8-8	0.089	3.17×10^7	0.85	20.9	0.85	1.86	1.13	35.45	1.45	2.06
GIN8-16	0.112	2.46×10^7	0.64	12.52	0.51	1.41	0.83	20.32	0.83	1.56

Table 3- Summary of effective textural parameters for the calculation of the decompression rates (dP/dt) according to Eq.1 (see text for explanation). VND_{eff} is calculated for the vesicle size at Modal length L (cf. Fig. 4) and result in an effective water content ($H2O_{eff}$), an effective pressure (P_{eff}) and depth (h_{eff}). Calculations have been performed at starting H2O wt% of 1.33 and 1.95 (see text for explanation.

It must be noted that these values are very close to the total VND (Fig. 3; Tables 2, 3), as typical for homogeneous bubble nucleation (cf Mourtada-Bonnefoi and Laporte 2002). Considering the homogeneous bubble nucleation, the surface tensions σ is taken at 0.045 N m^{-1} (Shea 2017).

Results of the application for Equation 1 are reported in Table 3, Fig. 7 and Supplementary material SM5.

The obtained dP/dt values for 1.33wt% H_2O content range between 0.43 MPa s^{-1} and 2.18 MPa s^{-1} (GIN1-4 and GIN8-4 respectively; Fig. 7). These values increase up to 0.48 and 2.49 MPa s^{-1} for 1.95wt% H_2O content (GIN1-4 and GIN8-4 respectively; Fig. 7). These value ranges overlap with those calculated by Georgeais et al. (2025). Such wide ranges of values are a measure of the uncertainties in inverting textural data to decompression rates, but they provide

a first order assessment which is useful especially where, like in the case of the July 3rd, 2019, eruption, there are other independent observables to compare with. Decompression rates convert to a range of average minimum (for LP foam density of 1000 kg m^{-3}) and average maximum (for LP density of 2776 kg m^{-3}) uprise velocities of the LP magma of 50-140 m s^{-1} (Table 3; Supplementary material SM7). These velocities agree with those calculated above from the July 3rd, 2019, mass eruption rate and much higher than those reported in the literature (Ripepe et al., 2021; Pichavant et al., 2022), consistent with the conduit having been "opened" by the initial blast. The closest values (at the lower end of our estimates) have been calculated in Valdivia et al., (2023), who emphasised the role of the very low viscosity of the LP magma in allowing very fast ascent rates. At such ascent rates, bubbles in the range of those measured in the LP pumice lapilli remain inside the melt as their Stokes numbers are small. This allows a closed-system degassing and foaming of the LP ascending magma, resulting in the upward decrease in density to values measured in the pumice lapilli (600-1000 kg m^{-3}).

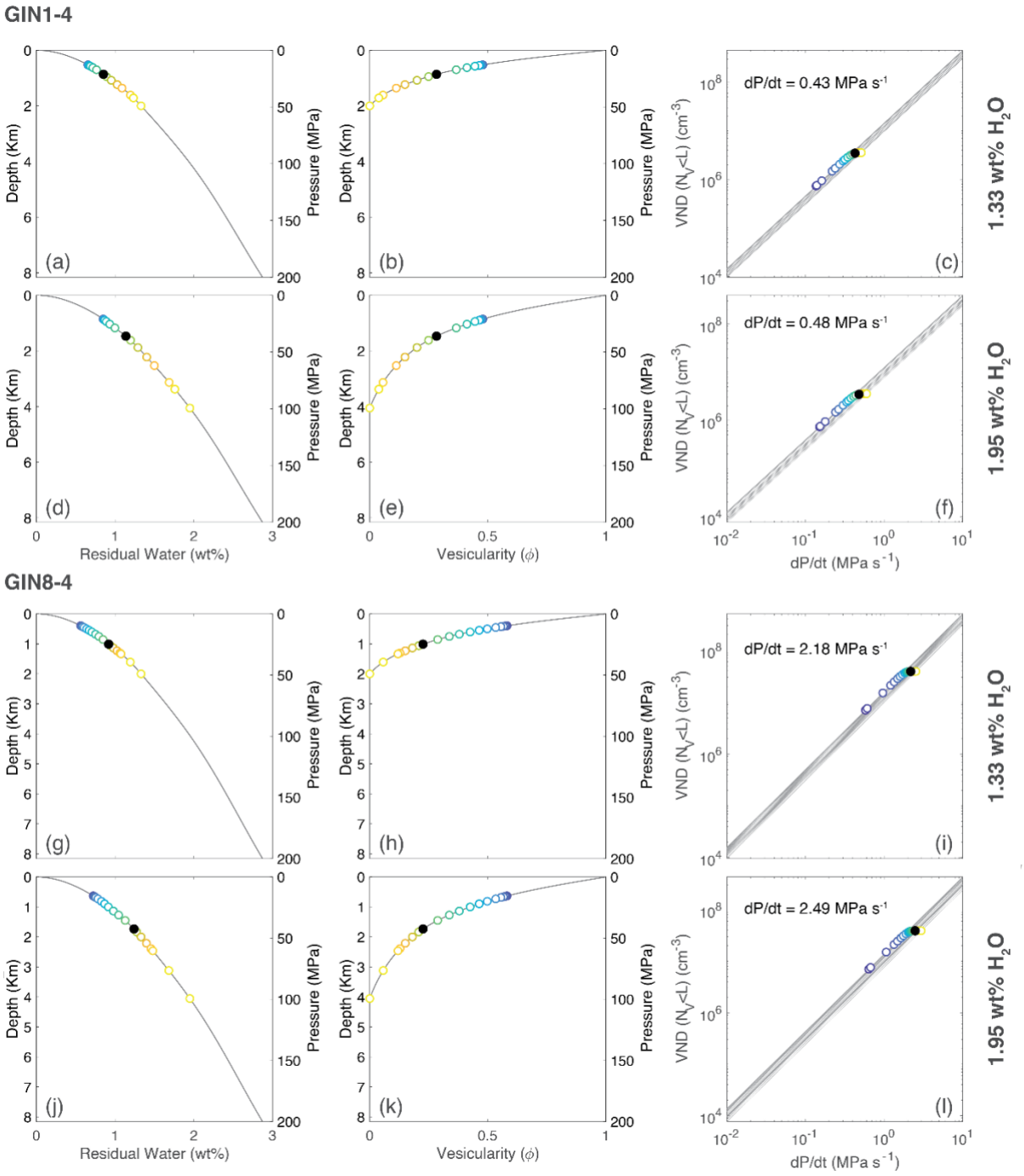

Fig. 7 – Residual water, vesicularity and decompression rates (dP/dt) derived from textural data for samples GIN1-4 and GIN8-4, for the selected initial water content scenarios of 1.33wt% and 1.95wt% (see text for explanation).

We applied the model of La Spina et al., (2022) to verify the dynamics of the LP magma mobilization from depths comprised between 2.5 and 5 km. The initial conditions were set with the first 2.5 km of the conduit filled by HP magma. The full set of initial parameters is summarized in Supplementary material SM8. We have simulated different driving pressures

necessary to fully evacuate the HP magma from the conduit. The results for the consequent uprise of the LP magma are reported in Fig. 8. The numerical solutions are obtained using a shooting technique, which consists of searching for the initial magma ascent velocity that satisfies the boundary condition at the volcanic vent, where the pressure equals atmospheric pressure, that are the conditions envisaged following the initial blast for the rise of the LP plume (Fig. 6b). The pressure range (120–190 MPa) reflects the physical limitations of the model. For bottom pressures below 110 MPa, no solution is possible, as the inlet pressure is insufficient to drive the stiff HP magma to the surface. Conversely, for pressures above 200 MPa, the results become physically inconsistent.

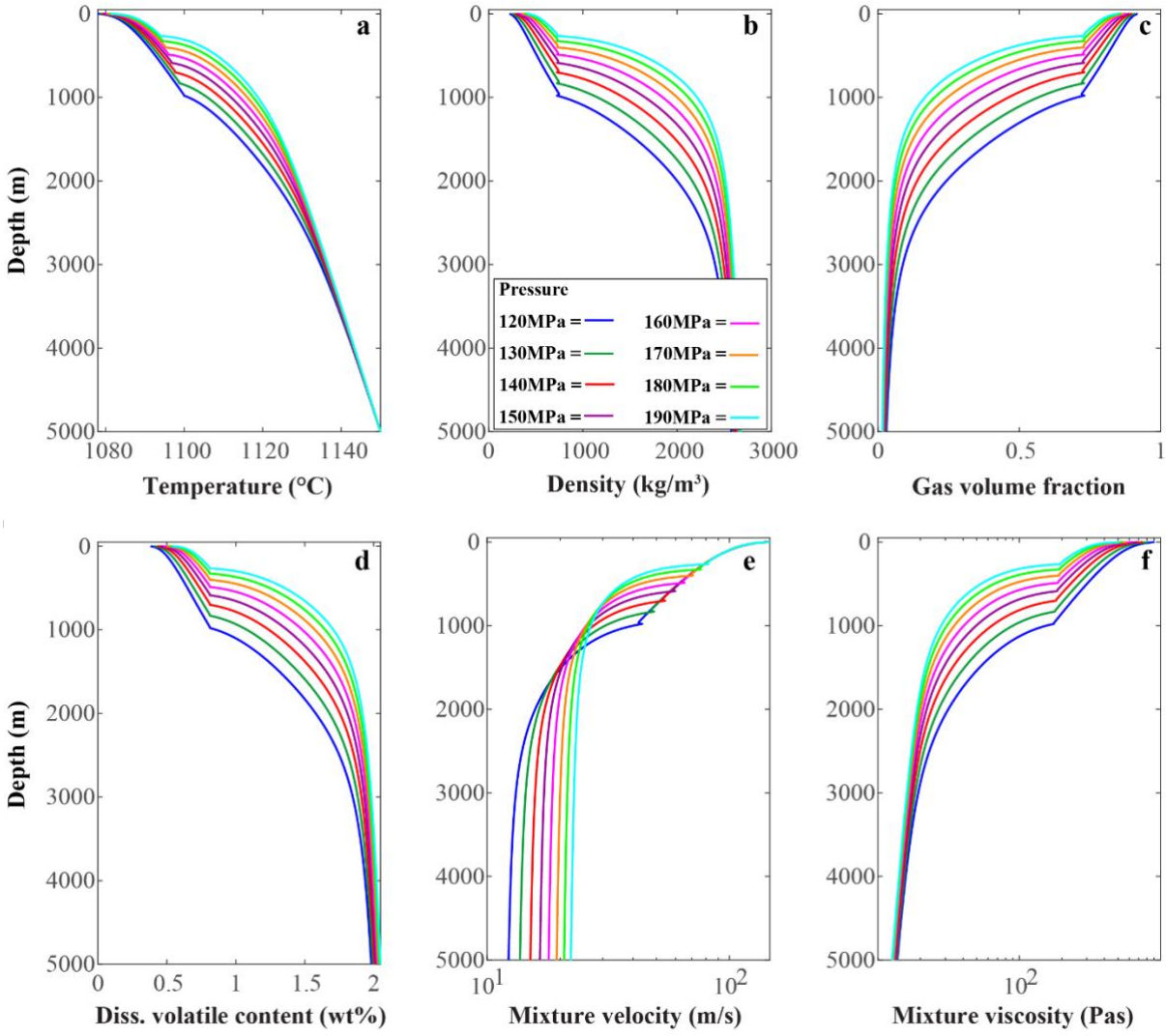

Figure 8: Temperature (a), density (b) gas volume fraction (c), dissolved volatile content (d), mixture velocity (e) and mixture viscosity (f) shown as a function of depth. These results are computed using a volume fraction criterion for magma fragmentation, with a threshold of ~85 vol %. The viscosity model proposed by Valdivia et al., (2023) is applied, assuming constant crystal content.

The results show that the pressure at the bottom of the conduit strongly influences the ascent dynamics of the LP magma. Before reaching the fragmentation level, ascent velocities fall within a range of approximately 44 to 82 m s^{-1}, depending on the bottom pressure. Above the fragmentation level, velocities increase significantly, reaching exit velocities at the vent of 142-147 m s^{-1} (Fig. 8e).

During ascent, temperature decreases (Fig. 8a), and density drops significantly due to volatile exsolution and foaming (Fig. 8b). Dissolved volatiles (Fig. 8d) decrease rapidly near the fragmentation level, causing a marked increase in the gas volume fraction (Fig. 8c). The fragmentation level, marked by a slope change in the curves, represents the transition to a gas-particle mixture. This occurs at depths of approximately 1 km for a driving pressure of 120 MPa and 260 meters for a driving pressure of 190 MPa.

Although the mass flow rate is not explicitly shown, it falls within the range of 6×10^5 to 1.2×10^6 kg s^{-1}, depending on the driving pressure.

The modeling results are in excellent agreement with the textural and observational calculations presented above for the July 3rd, 2019, LP pumice and could be easily achieved in a Vulcanian scenario. In contrast, even the highest calculated and modelled uprise velocities could not be reconciled with the "standard model". According to literature, this model involves the buoyant rise of a small blob of volatile-rich LP magma (10^3-10^4 m^3) from depths of 7-10 km through the LP magma already present in the plumbing system, reaching the LP-HP transition at rise speed of 1-2 m s^{-1} (e.g. Pichavant et al., 2022). The momentum from this ascent is then proposed to displace the HP magma in the shallow conduit (Métrich et al., 2010, 2021; Bertagnini et al., 2011). Using Poiseuille's law $Qv = \frac{\pi R^4 \Delta p}{8 \mu L}$, we calculated the driving pressure (Δp) required for the LP magma batch to displace the HP magma in a 2-km-long conduit (L; Fig. 6a), with a radius (R) of 2.5 m, and viscosity (μ) of 10^3 and 10^4 Pa s (Métrich et al., 2001; Burton et al., 2007; Vona et al., 2011; Gurioli et al., 2014), at the observed Q_v of 3.85 x 10^3 m^3 s^{-1} (Giordano and De Astis 2021). The resulting driving pressure needed to displace the static HP magma is comprised between 5 x 10^7 and 5 x 10^8 Pa, which agrees with our modeling and which corresponds to a force F ((Δp) times the cross-sectional area of the conduit) of ~10^9-10^{10} N. As the evacuation of the HP magma mass (m = 7×10^7 kg) lasted approximately 12 s (Giordano and De Astis, 2021), we estimate the velocity (v) of the LP

magma batch upon elastic impact at the base of the HP conduit using the impulse theorem, $v = \frac{F\,\Delta t}{2\,m}$. This approach yields unrealistically high ascent velocities on the order of 10^2–10^3 m s^{-1}. Notably, assuming a purely elastic impact is also highly unrealistic, as the "standard model" suggests that LP magma should be vesicular and therefore compressible.

These findings indicate that the "standard model" is physically unviable, and that the ascent of a small LP magma batch at 1-2 m s^{-1} (Pichavant et al., 2022) cannot push and displace the HP magma resident in the shallow conduit and therefore cannot act as the short-term (minutes-scale) trigger for Vulcanian explosions at Stromboli.

Conversely, the rise of discrete, small LP magma batches should stop at the HP-LP transition, well explaining the long-term processes of magma transfer within the deep system (Caricchi et al. 2024), where their accumulation at the HP-LP transition (and/or at kinks of the conduit geometry) probably leads to its dynamic and temporary shallowing, through processes of mingling and mixing (Fig. 6a). Furthermore, the accumulation of these LP magma batches over time may explain the segregation and upward migration of progressively larger gas slugs (Fig. 6a), possibly tracked by the increase over time of VLP size (Giudicepietro et al. 2020, 2022).

We remark that all available geophysical data indicate that the pre-eruptive pressure source and fragmentation level were located at very shallow depths (Figs 1b and 6a), within the HP magma, without any significant pre-explosion evacuation of the shallow conduit, ruling out the possibility that an LP magma batch rose through the HP-filled conduit.

We are fully aware that all calculations presented above are affected by significant uncertainties, such as those associated with the unknown conduit geometry at depth (cf. Viccaro et al., 2021). However, at first order, observations and textural data for the July 3rd, 2019, eruption point to a cascading top-down decompression event affecting only a small volume of the LP magma accumulated below the HP-LP transition in the months-days/hours before the eruption, as opposed to its fast active rise from much farther deep.

In summary, we propose an alternative conceptual model to explain Vulcanian eruptions at open conduit basaltic volcanoes, such as those that occur at Stromboli. This model involves the prolonged build-up over months to hours, as described by previous studies (e.g. Métrich et al., 2021; Aiuppa et al., 2021; Petrone et al 2022; Caricchi et al., 2024; Stix et al., 2025) during which an increase in magma influx from depth was not compensated by magma outflux,

accumulating magma within the plumbing system (Laiolo et al., 2022). During this prolonged period, small CO_2-rich LP magma batches are progressively transported upward from several kilometers depth, where they stop at the HP-LP transition. This process hybridizes magma between 4 km and 2 km (cf. Landi et al., 2022), dynamically shifting the HP-LP transition upward, leading to the formation of a foam layer at the transition (Woods and Cardoso 1997; Phillips and Woods, 2001; Mattia et al., 2021; Caricchi et al., 2024) (Fig. 6a). Passive CO_2-rich gas leakage from the foam would be the mechanism causing the precursory CO_2 flux increase observed over timescales of days/weeks (Aiuppa et al., 2021). The fate of these predisposing conditions, i.e. whether toward effusive or explosive styles and at what intensity, are instead controlled by short-term processes in the upper part of the conduit, especially in response to pressurization and failure of the shallow HP magma. The formation and upward migration of a large gas slug can induce the sudden increase of the gas flux through the HP magma-filled conduit beyond its permeability (Fig. 6a; cf. Allard, 2010; Aiuppa et al., 2021) possibly enhanced by kinks in the shallow conduit geometry (Viccaro et al., 2021; Fig. 6b). GBInSAR data may suggest that the process of pressurization at the base of the shallow conduit started a couple of hours before the eruption (Di Traglia et al., 2021), but the upward migration of the gas slug and its expansion within the last few hundreds of meters of HP-filled conduit accelerated suddenly just few minutes before the blast (Di Lieto et al. 2020; Giudicepietro et al. 2020; Ripepe et al., 2021; Viccaro et al., 2021). This explains the rapid pressurization of the HP magma and shallow failure/blasting of the vent, resulting in the short-lived, Vulcanian eruption observed at Stromboli (Fig. 1). Similar to more felsic Vulcanian eruptions, the sudden failure and evacuation of the shallow HP magma generate a downward-propagating rarefaction wave (Woods, 1995). This decompression wave triggers first the withdrawal of the remaining HP magma and then the closed-system degassing, foaming, rapid ascent, and explosive fragmentation of the deeper LP magma, with the eruption ceasing once the magmastatic pressure is restored in the conduit (Fig. 6b).

We propose that the “gas slug model” provides a more comprehensive explanation for the wealth of data and observations for the July 3rd, 2019, eruption at Stromboli. We note that the phenomenology and deposit types of all other “paroxysmal” eruptions occurred at Stromboli share very similar characteristics, so we suggest that the gas slug model may have a general applicability. For example, fast and shallow pre-eruptive inflation patterns similar to what occurs at Stromboli are observed elsewhere prior to Vulcanian explosions, such as at Sakurajima, Suwanosejima (Japan), and Semeru (Indonesia), also interpreted as the separation

of a gas slug and the pressurization of the shallow magma plug (Iguchi et al., 2008; Kazahaya et al., 2016). The gas slug model supports adopting the term “basaltic Vulcanian” to describe the eruption style shown by the July 3rd, 2019, Stromboli eruption and similar occurrences (Giordano et al., 2024), replacing the currently vague and non-descriptive term “paroxysm”. We also concur with Giordano and De Astis (2021) that “basaltic Vulcanian”, akin to “basaltic Plinian”, offers a classification that effectively highlights both the similarities and distinctions between eruptions styles at felsic and mafic volcanoes. This term emphasizes key characteristics such as the sudden release of gas overpressure, the top-down decompression of the magma in the conduit, and the short-lived, impulsive nature of these eruptions and their associated phenomena, which are comparable with classic Vulcanian eruptions (Self et al., 1978; Turcotte et al., 1990; Woods, 1995; Stix et al., 1997; Clarke et al., 2002; 2015; Fromenti et al., 2003; Iguchi et al. 2008; Kazahaya et al., 2016).

Additionally, this classification is advantageous as it distinguishes these eruptions from other explosive styles at mafic volcanoes also often addressed as paroxysmal (e.g. fire fountains and violent strombolian eruptions), easing the communication about these different kinds of eruption styles among scientists and to the public, and clarifying their unique genetic mechanisms and the different expected precursory phenomena.

In this regard, our study demonstrates that it is essential to distinguish between: i) long-term (month to hours) build up processes and the related monitoring signals that record the increase in magma influx in the plumbing system not compensated by magma outflux, and ii) the short-term (minutes) processes and the related monitoring signals that track the gas slug-driven pressurization of the HP magma in the shallow conduit and the onset of the Vulcanian eruption controlled by the blasting of the vent and subsequent top down decompression of the HP-LP magma resident in the rest of the conduit. We highlight that the short-lived nature of the eruption is associated with the fast restoration of near-magmastatic conditions once the conduit is re-filled.

We suggest focussing future research on the identification of robust precursors of basaltic Vulcanian eruptions which anticipate the final short term (minutes) inflation of the summit cone. Specifically, it is critical to search for geophysical and geochemical evidence of processes associated with formation and collapse of LP foam layers of different sizes, taking into account also the possible role of the geometry of the plumbing system. If recognized, these monitoring signals may herald the rise of large gas slugs through the magma column.

Additionally, it is important to monitor processes of densification of the shallow HP weak plug which may modulate the permeability threshold and the timing and extent of pressurization of the shallow conduit (cf. Clarke et al., 2002).

5 Conclusions

The classification and nomenclature of eruption styles remain fundamental components of volcanology. They not only ensure precise description of eruptive phenomena but also provide a conceptual framework for interpreting monitoring signals and effectively communicating hazards to civil protection and exposed populations.

This study demonstrates why the term 'paroxysm', traditionally used at Stromboli to describe its most intense explosions, is ambiguous and inconsistent with the eruption style it signifies. We argue that these events align more closely with Vulcanian eruptions, distinctly different from other explosive basaltic eruption styles, such as fire fountains and violent Strombolian eruptions.

Using textural data of the low porphyritic basaltic pumice from the July 3, 2019, eruption, we reconstructed and modelled the conduit processes, from bubble nucleation to fragmentation. These processes were examined within the context of existing literature, distinguishing between long-term (months to days/hours) precursory buildup processes, best evidenced by gas geochemistry and mineral chemistry, and short-term precursory processes (minutes), which are captured through pyroclast textures and geophysics. The proposed short-term term mechanism for the eruption involves the overpressurization of the HP magma filling the shallow conduit as a result of the arrival of a large gas slug. This gas convoy likely forms as a result of foam collapse in the lower, LP magma-dominated portion of the conduit (> 2 km depth), where, once formed, the gas slug migrates “silently”, likely due to the very low viscosity of the LP magma. Upon reaching the upper 2 km, where the conduit is filled by highly porphyritc (HP), more viscous magma, the slug forces the gas through the resident HP magma exceeding its percolation threshold, leading to its progressive and upward overpressurisation within minutes. This fast process of pressurization, lasting minutes, is witnessed by geophysical monitoring data and constrained within the shallowest 650 m of conduit. The conduit then fails at few tens of metres below the vent releasing the gas overpressure, causing shockwaves, ballistic ejection, vent flaring, and pyroclastic flows. The rapid removal of HP

magma from the shallow conduit induces a downward propagating decompression wave, triggering the full withdrawal of the remaining HP magma and the vesiculation and upward acceleration of deeper LP magma. This LP magma rises (and partly mingles with the HP magma) as a closed degassing system, potentially reaching ascent velocities at fragmentation level of up to ~100 m s^{-1}. This sudden process explains the fragmentation of microlite-free basaltic pumice derived from the stored LP magma. The eruption terminates once the shallow conduit, near-magmastatic pressure is restored, as no further overpressure remains in the system. This accounts for the short duration of the eruption and limited erupted volume.

The proposed conceptual model aligns with the Vulcanian eruption style, with the adjective 'basaltic' to distinguish the conduit processes specific to open-conduit basaltic volcanoes from those associated with gas pressurization at more felsic and closed-conduit volcanoes.

Within this framework, the traditional classification of ordinary Strombolian, major and paroxysmal eruptions at Stromboli should be reappraised. These events represent a continuum from Strombolian to basaltic Vulcanian eruption, driven by progressively larger gas slugs pressurizing the shallow conduit, in agreement with the localization of the pressure sources for geophysical signals (cf. Ripepe et al., 2021; Calvari et al., 2021). The extent to which the LP magma is involved in the Vulcanian explosions (major and paroxysmal explosions) depends on the amount of HP magma evacuated from the shallow conduit, which is proportional to the extent of decompression affecting the near-static magmatic column.

This gas slug-driven basaltic Vulcanian conceptual model for the occasional large explosions at Stromboli provides a robust framework for investigating and understanding the precursory monitoring signals compared to the mainstream model of rapid LP magma ascent from far deeper reservoirs.

In addition, adopting the term "Vulcanian" would facilitate clearer communication of eruption characteristics to stakeholders, including civil authorities, scientists, including tourists. This classification takes into account the expected phenomena of these eruptions enhancing understanding and preparedness.

Acknowledgements

GG and AV acknowledge the grant to the Department of Science, Roma Tre University (MIUR-Italy Dipartimenti di Eccellenza, ARTICOLO 1,COMMI 314–337 LEGGE 232/2016). AV acknowledge funding by the European Union–Next Generation EU, National Recovery and Resilience Plan Mission 4-Component 2. Project P20222BP7J. DDG acknowledges the funding from the European Research Council (ERC) under the European Union's Horizon Europe research and innovation programme (NANOVOLC, ERC Consolidator Grant – No. 101044772). DDG also acknowledges the Deutsche Forschungsgemeinschaft (DFG) project DI 2751/2–1 and funding from the European Union's – Next Generation EU, Missione 4 Componente 1 CUP B53D23007230006. Dante Arteaga (Instituto de Geociencias-UNAM) processed the 3D microtomographs. The INGV electron microscope laboratory at the Osservatorio Vesuviano have been financially supported by the EPOS Research Infrastructure through the contribution of the Italian Ministry of University and Research (MUR). The authors would like to acknowledge J. Stix and F. Di Traglia for their very constructive reviews.

References

1. Abbruzzese D (1935) Sulla catastrofica esplosione dello Stromboli dell'11 settembre 1930. Gioenia Proc Soc Nat Sci 1:1–13
2. Aiuppa A, Burton M, Allard P, Caltabiano T, Giudice G, Gurrieri S, Liuzzo M, Salerno G (2011) First observational evidence for the CO2-driven origin of Stromboli's major explosions. Solid Earth 2:135–142. https:// doi. org/ 10. 5194/ se-2- 135- 2011
3. Aiuppa, A., Bitetto, M., Delle Donne, D., La Monica, F.P., Tamburello, G., Coppola, D., Della Schiava, M., Innocenti, L., Lacanna, G., Laiolo, M., Massimetti, F., Pistolesi, M., Silengo, M.C., Ripepe, M., 2021. Volcanic CO_2 tracks the incubation period of basaltic paroxysms. Sci. Adv. 7, eabh0191. https://doi.org/10.1126/sciadv.abh0191
4. Allard, P., 2010. A CO2-rich gas trigger of explosive paroxysms at Stromboli basaltic volcano, Italy. Journal of Volcanology and Geothermal Research 189, 363–374. https://doi.org/10.1016/j.jvolgeores.2009.11.018
5. Andronico, D., Del Bello, E., D'Oriano, C., Landi, P., Pardini, F., Scarlato, P., De' Michieli Vitturi, M., Taddeucci, J., Cristaldi, A., Ciancitto, F., Pennacchia, F., Ricci, T., Valentini, F., 2021. Uncovering the eruptive patterns of the 2019 double paroxysm eruption crisis of Stromboli volcano. Nat Commun 12, 4213. https://doi.org/10.1038/s41467-021-24420-1
6. Arzilli, F., La Spina, G., Burton, M.R., Polacci, M., Le Gall, N., Hartley, M.E., Di Genova, D., Cai, B., Vo, N.T., Bamber, E.C., Nonni, S., Atwood, R., Llewellin, E.W., Brooker, R.A., Mader, H.M., Lee, P.D., 2019. Magma fragmentation in highly explosive basaltic eruptions induced by rapid crystallization. Nat. Geosci. 12, 1023–1028. https://doi.org/10.1038/s41561-019-0468-6
7. Barberi, F. Rosi, M. Sodi A. (1993). "Volcanic hazard assessment at Stromboli based on review of historical data". Acta Vulcanologica, 3, 173-187
8. Bertagnini, A., Di Roberto, A., Pompilio, M., 2011. Paroxysmal activity at Stromboli: lessons from the past. Bull Volcanol 73, 1229–1243. https://doi.org/10.1007/s00445-011-0470-3
9. Bertagnini, A., Métrich, N., Francalanci, L., Landi, P., Tommasini, S., Conticelli, S., 2008. Volcanology and Magma Geochemistry of the Present-Day Activity: Constraints on the Feeding System, in: Calvari, S., Inguaggiato, S., Puglisi, G., Ripepe, M., Rosi, M. (Eds.), Geophysical Monograph Series. American Geophysical Union, Washington, D. C., pp. 19–37. https://doi.org/10.1029/182GM04
10. Bertagnini, A., Métrich, N., Landi, P., Rosi, M., 2003. Stromboli volcano (Aeolian Archipelago, Italy): An open window on the deep-feeding system of a steady state basaltic volcano. J. Geophys. Res. 108, 2002JB002146. https://doi.org/10.1029/2002JB002146
11. Bevilacqua, A., Bertagnini, A., Pompilio, M. *et al.,* Major explosions and paroxysms at Stromboli (Italy): a new historical catalog and temporal models of occurrence with uncertainty quantification. *Sci Rep* **10**, 17357 (2020). https://doi.org/10.1038/s41598-020-74301-8
12. Bevilacqua, A., Bertagnini, A., Pompilio, M., Landi, P., Del Carlo, P., Di Roberto, A., Aspinall, W., Neri, A., 2020. Major explosions and paroxysms at Stromboli (Italy): a

new historical catalog and temporal models of occurrence with uncertainty quantification. Sci Rep 10, 17357. https://doi.org/10.1038/s41598-020-74301-8

13. Bisson, M., Spinetti, C., Gianardi, R., Strehlow, K., De Beni, E., Landi, P., 2023. High-resolution mapping and dispersion analyses of volcanic ballistics emitted during the 3rd July 2019 paroxysm at Stromboli. Sci Rep 13, 13465. https://doi.org/10.1038/s41598-023-39600-w
14. Blower, J.D., Mader, H.M., Wilson, S.D.R., 2001. Coupling of viscous and diffusive controls on bubble growth during explosive volcanic eruptions. Earth and Planetary Science Letters 193, 47–56. https://doi.org/10.1016/S0012-821X(01)00488-5
15. Bonaccorso, A., Gambino, S., Guglielmino, F., Mattia, M., Puglisi, G., Boschi, E., 2008. Stromboli 2007 eruption: Deflation modeling to infer shallow-intermediate plumbing system. Geophysical Research Letters 35, 2007GL032921. https://doi.org/10.1029/2007GL032921
16. Bonechi, B., Polacci, M., Arzilli, F., La Spina, G., Hazemann, J.-L., Brooker, R.A., Atwood, R., Marussi, S., Lee, P.D., Wogelius, R.A., Fellowes, J., Burton, M.R., 2024. Direct observation of degassing during decompression of basaltic magma. Sci. Adv. 10, eado2585. https://doi.org/10.1126/sciadv.ado2585
17. Burton, M., Allard, P., Muré, F., La Spina, A., 2007. Magmatic Gas Composition Reveals the Source Depth of Slug-Driven Strombolian Explosive Activity. Science 317, 227–230. https://doi.org/10.1126/science.1141900
18. Calvari, S., Cannavò, F., Bonaccorso, A., Spampinato, L., Pellegrino, A.G., 2018. Paroxysmal Explosions, Lava Fountains and Ash Plumes at Etna Volcano: Eruptive Processes and Hazard Implications. Front. Earth Sci. 6, 107. https://doi.org/10.3389/feart.2018.00107
19. Calvari, S., Spampinato, L., Lodato, L., 2006. The 5 April 2003 vulcanian paroxysmal explosion at Stromboli volcano (Italy) from field observations and thermal data. Journal of Volcanology and Geothermal Research 149, 160–175. https://doi.org/10.1016/j.jvolgeores.2005.06.006
20. Calvari, S., Giudicepietro, F., Di Traglia, F., Bonaccorso, A., Macedonio, G., & Casagli, N. (2021). Variable magnitude and intensity of Strombolian explosions: Focus on the eruptive processes for a first classification scheme for Stromboli volcano (Italy). *Remote Sensing*, *13*(5), 944.
21. Caracciolo, A., Gurioli, L., Marianelli, P., Bernard, J., Harris, A., 2021. Textural and chemical features of a "soft" plug emitted during Strombolian explosions: A case study from Stromboli volcano. Earth and Planetary Science Letters 559, 116761. https://doi.org/10.1016/j.epsl.2021.116761
22. Cardone, M., Cannata, A., Giuffrida, M., Iozzia, A., Minio, V., Viccaro, M., Gambino, S., 2024. Changing magma recharge/discharge dynamics during the 2020–22 lava fountaining activity at Mt. Etna revealed by tilt deformation and volcanic tremor. Journal of Volcanology and Geothermal Research 449, 108074. https://doi.org/10.1016/j.jvolgeores.2024.108074
23. Caricchi, L., Montagna, C.P., Aiuppa, A., Lages, J., Tamburello, G., Papale, P., 2024. CO_2 Flushing Triggers Paroxysmal Eruptions at Open Conduit Basaltic Volcanoes. JGR Solid Earth 129, e2023JB028486. https://doi.org/10.1029/2023JB028486

24. Caricchi, L., Sheldrake, T.E., Blundy, J., 2018. Modulation of magmatic processes by CO2 flushing. Earth and Planetary Science Letters 491, 160–171. https://doi.org/10.1016/j.epsl.2018.03.042
25. Cas, R., Giordano, G., Wright, J.V., 2024. Influence of Environment on Magma Properties, Eruption Processes, and Deposits: How Different Ambient Environments (Atmosphere, Oceans/Lakes, Ice, and Lithosphere) Affect Volcanic Eruptions and Deposits, in: Volcanology. Springer International Publishing, Cham, pp. 75–114. https://doi.org/10.1007/978-3-319-66613-6_3
26. Cashman, K.V., Scheu, B., 2015. Magmatic Fragmentation, in: The Encyclopedia of Volcanoes. Elsevier, pp. 459–471. https://doi.org/10.1016/B978-0-12-385938-9.00025-0
27. Chouet, B., Dawson, P., Martini, M., 2008. Shallow-conduit dynamics at Stromboli Volcano, Italy, imaged from waveform inversions. SP 307, 57–84. https://doi.org/10.1144/SP307.5
28. Cimarelli, C., Di Traglia, F., Taddeucci, J., 2010. Basaltic scoria textures from a zoned conduit as precursors to violent Strombolian activity. Geology 38, 439–442. https://doi.org/10.1130/G30720.1
29. Civico, R., Ricci, T., Scarlato, P., Andronico, D., Cantarero, M., Carr, B.B., De Beni, E., Del Bello, E., Johnson, J.B., Kueppers, U., Pizzimenti, L., Schmid, M., Strehlow, K., Taddeucci, J., 2021. Unoccupied Aircraft Systems (UASs) Reveal the Morphological Changes at Stromboli Volcano (Italy) before, between, and after the 3 July and 28 August 2019 Paroxysmal Eruptions. Remote Sensing 13, 2870. https://doi.org/10.3390/rs13152870
30. Civico, R., Ricci, T., Cecili, A., Scarlato, P., 2024. High-resolution topography reveals morphological changes of Stromboli volcano following the July 2024 eruption. Sci Data 11, 1219. https://doi.org/10.1038/s41597-024-04098-y
31. Clarke, A. B., Voight, B., Neri, A., & Macedonio, G. (2002). Transient dynamics of vulcanian explosions and column collapse. *Nature*, *415*(6874), 897-901.
32. Clarke, A.B., Esposti Ongaro, T., Belousov, A., 2015. Vulcanian Eruptions, in: The Encyclopedia of Volcanoes. Elsevier, pp. 505–518. https://doi.org/10.1016/B978-0-12-385938-9.00028-6
33. Del Bello, E., Lane, S.J., James, M.R., Llewellin, E.W., Taddeucci, J., Scarlato, P., Capponi, A., 2015. Viscous plugging can enhance and modulate explosivity of strombolian eruptions. Earth and Planetary Science Letters 423, 210–218. https://doi.org/10.1016/j.epsl.2015.04.034
34. Di Carlo, I., 2006. Experimental Crystallization of a High-K Arc Basalt: the Golden Pumice, Stromboli Volcano (Italy). Journal of Petrology 47, 1317–1343. https://doi.org/10.1093/petrology/egl011
35. Di Fiore, F., Vona, A., Di Genova, D., Pontesilli, A., Calabrò, L., Mollo, S., Taddeucci, J., Romano, C., Scarlato, P., 2024. Magma titanium and iron contents dictate crystallization timescales and rheological behaviour in basaltic volcanic systems. Commun Earth Environ 5, 283. https://doi.org/10.1038/s43247-024-01452-1

36. Di Lieto, B., Romano, P., Scarpa, R., Linde, A.T., 2020. Strain Signals Before and During Paroxysmal Activity at Stromboli Volcano, Italy. Geophysical Research Letters 47, e2020GL088521. https://doi.org/10.1029/2020GL088521
37. Di Piazza, A., Vona, A., Mollo, S., De Astis, G., Soto, G.J., Romano, C., 2019. Unsteady magma discharge during the "El Retiro" subplinian eruption (Turrialba volcano, Costa Rica): Insights from textural and petrological analyses. Journal of Volcanology and Geothermal Research 371, 101–115. https://doi.org/10.1016/j.jvolgeores.2019.01.004
38. Di Stefano, F., Mollo, S., Ubide, T., Petrone, C.M., Caulfield, J., Scarlato, P., Nazzari, M., Andronico, D., Del Bello, E., 2020. Mush cannibalism and disruption recorded by clinopyroxene phenocrysts at Stromboli volcano: New insights from recent 2003–2017 activity. Lithos 360–361, 105440. https://doi.org/10.1016/j.lithos.2020.10544
39. Di Traglia, F., Cimarelli, C., De Rita, D., & Torrente, D. G. (2009). Changing eruptive styles in basaltic explosive volcanism: examples from Croscat complex scoria cone, Garrotxa Volcanic Field (NE Iberian Peninsula). *Journal of Volcanology and Geothermal Research*, *180*(2-4), 89-109.
40. Di Traglia, F., Calvari, S., D'Auria, L., Nolesini, T., Bonaccorso, A., Fornaciai, A., ... & Casagli, N. (2018). The 2014 effusive eruption at Stromboli: New insights from in situ and remote-sensing measurements. *Remote Sensing*, *10*(12), 2035.
41. Di Traglia, F., De Luca, C., Manzo, M., Nolesini, T., Casagli, N., Lanari, R., & Casu, F. (2021). Joint exploitation of space-borne and ground-based multitemporal InSAR measurements for volcano monitoring: The Stromboli volcano case study. *Remote Sensing of Environment*, *260*, 112441.
42. Esposti Ongaro, T., De' Michieli Vitturi, M., Cerminara, M., Fornaciai, A., Nannipieri, L., Favalli, M., Calusi, B., Macías, J., Castro, M.J., Ortega, S., González-Vida, J.M., Escalante, C., 2021. Modeling Tsunamis Generated by Submarine Landslides at Stromboli Volcano (Aeolian Islands, Italy): A Numerical Benchmark Study. Front. Earth Sci. 9, 628652. https://doi.org/10.3389/feart.2021.628652
43. Francalanci L, Bertagnini A, Métrich N, Renzulli A, Vannucci R, Landi P et al (2008) Mineralogical, geochemical, and isotopic characteristics of the ejecta from the 5 April 2003 paroxysm at Stromboli, Italy: inferences on the preeruptive magma dynamics. Am Geophys Union Geophys Monogr Ser 182:19–39
44. Francalanci, L., Lucchi, F., Keller, J., De Astis, G., Tranne, C.A., 2013. Chapter 13 Eruptive, volcano-tectonic and magmatic history of the Stromboli volcano (north-eastern Aeolian archipelago). Memoirs 37, 397–471. https://doi.org/10.1144/M37.13
45. Formenti, Y., Druitt, T. H., & Kelfoun, K. (2003). Characterisation of the 1997 Vulcanian explosions of Soufrière Hills Volcano, Montserrat, by video analysis. *Bulletin of Volcanology*, *65*(8), 587-605.
46. Georgeais, G., Moussallam, Y., Rose-Koga, E. F., Koga, K. T., Gurioli, L., Harris, A., ... & Pistolesi, M. (2025). Deeper, faster, stronger? Extreme magma ascent rates and explosive eruption metrics at Stromboli volcano (Italy). *Bulletin of Volcanology*, *88*(1), 2.
47. Ghiorso, M.S., Gualda, G.A.R., 2015. An H2O–CO2 mixed fluid saturation model compatible with rhyolite-MELTS. Contrib Mineral Petrol 169, 53. https://doi.org/10.1007/s00410-015-1141-8

48. Giordano, G., Cas, R., Wright, J.V., 2024. Explosive Eruption Styles, Columns, and Pyroclastic Fallout Deposits: Subaerial and Subaqueous, Dynamics, Deposit Characteristics and Classification, in: Volcanology. Springer International Publishing, Cham, pp. 519–691. https://doi.org/10.1007/978-3-319-66613-6_9
49. Giordano, G., De Astis, G., 2021. The summer 2019 basaltic Vulcanian eruptions (paroxysms) of Stromboli. Bull Volcanol 83, 1. https://doi.org/10.1007/s00445-020-01423-2
50. Giudicepietro, F., López, C., Macedonio, G., Alparone, S., Bianco, F., Calvari, S., De Cesare, W., Delle Donne, D., Di Lieto, B., Esposito, A.M., Orazi, M., Peluso, R., Privitera, E., Romano, P., Scarpato, G., Tramelli, A., 2020. Geophysical precursors of the July-August 2019 paroxysmal eruptive phase and their implications for Stromboli volcano (Italy) monitoring. Sci Rep 10, 10296. https://doi.org/10.1038/s41598-020-67220-1
51. Giudicepietro, F., Calvari, S., D'Auria, L., Di Traglia, F., Layer, L., Macedonio, G., ... & Esposito, A. M. (2022). Changes in the eruptive style of Stromboli volcano before the 2019 paroxysmal phase discovered through SOM clustering of seismo-acoustic features compared with camera images and GBInSAR data. Remote Sensing, 14(5), 1287
52. Giuffrida, M., Cardone, M., Zuccarello, F., Viccaro, M., 2023. Etna 2011–2022: Discoveries from a decade of activity at the volcano. Earth-Science Reviews 245, 104563. https://doi.org/10.1016/j.earscirev.2023.104563
53. Gonnermann, H.M., Manga, M., 2013. Dynamics of magma ascent in the volcanic conduit, in: Fagents, S.A., Gregg, T.K.P., Lopes, R.M.C. (Eds.), Modeling Volcanic Processes. Cambridge University Press, pp. 55–84. https://doi.org/10.1017/CBO9781139021562.004
54. Guardo, R., Bilotta, G., Ganci, G., Zuccarello, F., Andronico, D., & Cappello, A. (2024). Modeling fire hazards induced by volcanic eruptions: the case of Stromboli (Italy). *Fire*, *7*(3), 70.
55. Gurioli, L., Colo', L., Bollasina, A.J., Harris, A.J.L., Whittington, A., Ripepe, M., 2014. Dynamics of Strombolian explosions: Inferences from field and laboratory studies of erupted bombs from Stromboli volcano. JGR Solid Earth 119, 319–345. https://doi.org/10.1002/2013JB010355
56. Gurioli, L., Harris, A.J.L., Houghton, B.F., Polacci, M., Ripepe, M., 2008. Textural and geophysical characterization of explosive basaltic activity at Villarrica volcano. J. Geophys. Res. 113, 2007JB005328. https://doi.org/10.1029/2007JB005328
57. Harris, A., Ripepe, M., 2007. Temperature and dynamics of degassing at Stromboli. J. Geophys. Res. 112, 2006JB004393. https://doi.org/10.1029/2006JB004393
58. Holt, S.J., Carey, R.J., Houghton, B.F., Orr, T., McPhie, J., Feig, S., 2019. Eruption and fountaining dynamics of selected 1985–1986 high fountaining episodes at Kīlauea volcano, Hawai'i, from quantitative vesicle microtexture analysis. Journal of Volcanology and Geothermal Research 369, 21–34. https://doi.org/10.1016/j.jvolgeores.2018.11.011
59. Houghton, B.F., Gonnermann, H.M., 2008. Basaltic explosive volcanism: Constraints from deposits and models. Geochemistry 68, 117–140. https://doi.org/10.1016/j.chemer.2008.04.002

60. Houghton, B.F., Wilson, C.J.N., 1989. A vesicularity index for pyroclastic deposits. Bull Volcanol 51, 451–462. https://doi.org/10.1007/BF01078811
61. Iacono, F., Bisson, M., Spinetti, C., & Kwasnitschka, T. (2025). Wildfires Induced by Volcanic Activity at Stromboli Island during the 2019 Summer through Satellite and Drone Data. *Remote Sensing in Earth Systems Sciences*, *8*(2), 733-752.
62. Iguchi, M., Yakiwara, H., Tameguri, T., Hendrasto, M., & Hirabayashi, J. I. (2008). Mechanism of explosive eruption revealed by geophysical observations at the Sakurajima, Suwanosejima and Semeru volcanoes. *Journal of Volcanology and Geothermal Research*, *178*(1), 1-9.
63. Imbò G (1928) Parossismo di Stromboli nel settembre 1930. Bull Volcanol 5(1):177–185
64. INGV 2024 BOLLETTINO SETTIMANALE n.29/2024. STROMBOLI SETTIMANA DI RIFERIMENTO 08/07/2024 - 14/07/2024 (data emissione 16/07/2024)
65. Insinga, L., Voloschina, M., Marianelli, P., Bartolomeo, E., Bertagnini, A., Métrich, N., ... & Pistolesi, M. (2025). Magma source, pre-eruptive dynamics and timescales of major explosions at Stromboli volcano (Italy). *Bulletin of Volcanology*, *87*(9), 75.
66. James, M.R., Lane, S.J., Corder, S.B., 2008. Modelling the rapid near-surface expansion of gas slugs in low-viscosity magmas. SP 307, 147–167. https://doi.org/10.1144/SP307.9
67. Jaupart, C., Vergniolle, S., 1989. The generation and collapse of a foam layer at the roof of a basaltic magma chamber. J. Fluid Mech. 203, 347–380. https://doi.org/10.1017/S0022112089001497
68. Johnson, E.R., Wallace, P.J., Cashman, K.V., Granados, H.D., Kent, A.J.R., 2008. Magmatic volatile contents and degassing-induced crystallization at Volcán Jorullo, Mexico: Implications for melt evolution and the plumbing systems of monogenetic volcanoes. Earth and Planetary Science Letters 269, 478–487. https://doi.org/10.1016/j.epsl.2008.03.004
69. Kazahaya, R., Shinohara, H., Mori, T., Iguchi, M., & Yokoo, A. (2016). Pre-eruptive inflation caused by gas accumulation: Insight from detailed gas flux variation at Sakurajima volcano, Japan. *Geophysical Research Letters*, *43*(21), 11-219.
70. Kennedy, B., Spieler, O., Scheu, B., Kueppers, U., Taddeucci, J., Dingwell, D.B., 2005. Conduit implosion during Vulcanian eruptions. Geol 33, 581. https://doi.org/10.1130/G21488.1
71. Kokandakar, G.J., Ghodke, S.S., Rathna, K., More, L.B., Nagaraju, B., Bhosle, M.V., Kumar, K.V., 2018. Density, Viscosity and Velocity (Ascent Rate) of Alkaline Magmas. Journal of the Geological Society of India 91, 135–146. https://doi.org/10.1007/s12594-018-0827-8
72. La Spina, G., Burton, M., De' Michieli Vitturi, M., 2015. Temperature evolution during magma ascent in basaltic effusive eruptions: A numerical application to Stromboli volcano. Earth and Planetary Science Letters 426, 89–100. https://doi.org/10.1016/j.epsl.2015.06.015
73. La Spina, G., Burton, M., De' Michieli Vitturi, M., Arzilli, F., 2016. Role of syn-eruptive plagioclase disequilibrium crystallization in basaltic magma ascent dynamics. Nat Commun 7, 13402. https://doi.org/10.1038/ncomms13402

74. La Spina, G., Arzilli, F., Burton, M. R., Polacci, M., & Clarke, A. B. (2022). Role of volatiles in highly explosive basaltic eruptions. *Communications Earth & Environment*, *3*(1), 156.
75. Laiolo, M., Delle Donne, D., Coppola, D., Bitetto, M., Cigolini, C., Della Schiava, M., ... & Ripepe, M. (2022). Shallow magma dynamics at open-vent volcanoes tracked by coupled thermal and SO2 observations. Earth and Planetary Science Letters, 594, 117726.
76. Landi, P., Corsaro, R.A., Francalanci, L., Civetta, L., Miraglia, L., Pompilio, M., Tesoro, R., 2009. Magma dynamics during the 2007 Stromboli eruption (Aeolian Islands, Italy): Mineralogical, geochemical and isotopic data. Journal of Volcanology and Geothermal Research 182, 255–268. https://doi.org/10.1016/j.jvolgeores.2008.11.010
77. Landi, P., D'Oriano, C., Petrelli, M., Nazzari, M., Andronico, D., 2022. Inferences on the magmatic plumbing system at Stromboli volcano (Italy) from trace element geochemistry of matrix glasses and minerals in different types of explosive eruptions. Contrib Mineral Petrol 177, 96. https://doi.org/10.1007/s00410-022-01962-1
78. Landi, P., Francalanci, L., Pompilio, M., Rosi, M., Corsaro, R.A., Petrone, C.M., Nardini, I., Miraglia, L., 2006. The December 2002–July 2003 effusive event at Stromboli volcano, Italy: Insights into the shallow plumbing system by petrochemical studies. Journal of Volcanology and Geothermal Research 155, 263–284. https://doi.org/10.1016/j.jvolgeores.2006.03.032
79. Langhammer, D., Di Genova, D., Steinle-Neumann, G., 2022. Modeling Viscosity of Volcanic Melts With Artificial Neural Networks. Geochem Geophys Geosyst 23, e2022GC010673. https://doi.org/10.1029/2022GC010673
80. Lautze, N.C., Houghton, B.F., 2005. Physical mingling of magma and complex eruption dynamics in the shallow conduit at Stromboli volcano, Italy. Geol 33, 425. https://doi.org/10.1130/G21325.1
81. Leduc, L., Gurioli, L., Harris, A., Colò, L., Rose-Koga, E.F., 2015. Types and mechanisms of strombolian explosions: characterization of a gas-dominated explosion at Stromboli. Bull Volcanol 77, 8. https://doi.org/10.1007/s00445-014-0888-5
82. Lucchi, F., Keller, J., De Astis, G., Francalanci, L., Tranne, C.A., 2013. Geological map of Stromboli, scale 1:10 000 (Aeolian archipelago). GBR.
83. Mangan, M.T., Cashman, K.V., 1996. The structure of basaltic scoria and reticulite and inferences for vesiculation, foam formation, and fragmentation in lava fountains. Journal of Volcanology and Geothermal Research 73, 1–18. https://doi.org/10.1016/0377-0273(96)00018-2
84. Mangan, M.T., Cashman, K.V., Swanson, D.A., 2014. The dynamics of Hawaiian-style eruptions: A century of study, Characteristics of Hawaiian Volcanoes. U.S. Geological Survey Professional Paper, 1801-8.
85. Marsh, J., Edmonds, M., Houghton, B., Buisman, I., Herd, R., 2024. Magma mingling during the 1959 eruption of Kīlauea Iki, Hawai'i. Bull Volcanol 86, 57. https://doi.org/10.1007/s00445-024-01748-2
86. Mattia, M., Di Lieto, B., Ganci, G., Bruno, V., Romano, P., Ciancitto, F., De Martino, P., Gambino, S., Aloisi, M., Sciotto, M., Scarpa, R., Ferlito, C., 2021. The 2019 Eruptive Activity at Stromboli Volcano: A Multidisciplinary Approach to Reveal Hidden Features

of the "Unexpected" 3 July Paroxysm. Remote Sensing 13, 4064. https://doi.org/10.3390/rs13204064

87. Mercalli, G., and Silvestri, O., 1891, L'eruzione dell'Isola di Vulcano incominciata il 3 agosto 1888 e terminata il 22 marzo 1890: Annali dell'ufficio Centrale di Meteorologia e Geodinamica , v. 10p. 71–281.
88. Métrich, N., Bertagnini, A., Di Muro, A., 2010. Conditions of Magma Storage, Degassing and Ascent at Stromboli: New Insights into the Volcano Plumbing System with Inferences on the Eruptive Dynamics. Journal of Petrology 51, 603–626. https://doi.org/10.1093/petrology/egp083
89. Métrich, N., Bertagnini, A., Landi, P., Rosi, M., Belhadj, O., 2005. Triggering mechanism at the origin of paroxysms at Stromboli (Aeolian Archipelago, Italy): The 5 April 2003 eruption. Geophysical Research Letters 32, 2004GL022257. https://doi.org/10.1029/2004GL022257
90. Métrich, N., Bertagnini, A., Pistolesi, M., 2021. Paroxysms at Stromboli Volcano (Italy): Source, Genesis and Dynamics. Front. Earth Sci. 9, 593339. https://doi.org/10.3389/feart.2021.593339
91. Misiti, V., Vetere, F., Mangiacapra, A., Behrens, H., Cavallo, A., Scarlato, P., Dingwell, D.B., 2009. Viscosity of high-K basalt from the 5th April 2003 Stromboli paroxysmal explosion. Chemical Geology 260, 278–285. https://doi.org/10.1016/j.chemgeo.2008.12.023
92. Mitchell, S.J., Fauria, K.E., Houghton, B.F., Carey, R.J., 2021. Sink or float: microtextural controls on the fate of pumice deposition during the 2012 submarine Havre eruption. Bull Volcanol 83, 80. https://doi.org/10.1007/s00445-021-01497-6
93. Montanaro C, Mick E, Salas-Navarro J, Caudron C, Cronin SJ, de Moor JM, Scheu B, Stix J, Strehlow K (2022) Phreatic and hydrothermal eruptions: from overlooked to looking over. Bull Volcanol 84:64. https://doi.org/10.1007/s00445-022-01571-7
94. Mourtada-Bonnefoi, C.C., Laporte, D., 2002. Homogeneous bubble nucleation in rhyolitic magmas: An experimental study of the effect of H_2O and CO_2. J. Geophys. Res. 107. https://doi.org/10.1029/2001JB000290
95. Namiki, A., Manga, M., 2008. Transition between fragmentation and permeable outgassing of low viscosity magmas. Journal of Volcanology and Geothermal Research 169, 48–60. https://doi.org/10.1016/j.jvolgeores.2007.07.020
96. Oppenheimer, J., Capponi, A., Cashman, K.V., Lane, S.J., Rust, A.C., James, M.R., 2020. Analogue experiments on the rise of large bubbles through a solids-rich suspension: A "weak plug" model for Strombolian eruptions. Earth and Planetary Science Letters 531, 115931. https://doi.org/10.1016/j.epsl.2019.115931
97. Parfitt, E.A., 2004. A discussion of the mechanisms of explosive basaltic eruptions. Journal of Volcanology and Geothermal Research 134, 77–107. https://doi.org/10.1016/j.jvolgeores.2004.01.002
98. Patanè, D., M. Mattia, G. Di Grazia, F. Cannavò, E. Giampiccolo, C. Musumeci, P. Montalto, and E. Boschi (2007), Insights into the dynamic processes of the 2007 Stromboli eruption and possible meteorological influences on the magmatic system, Geophys. Res. Lett., 34, L22309, doi:10.1029/2007GL031730.

99. Patanè, D., Barberi, G., De Gori, P., Cocina, O., Zuccarello, L., Garcia-Yeguas, A., Castellano, M., D'Alessandro, A., Sgroi, T., 2017. The shallow magma chamber of Stromboli Volcano (Italy). Geophysical Research Letters 44, 6589–6596. https://doi.org/10.1002/2017GL073008
100. Patrick, M.R., Harris, A.J.L., Ripepe, M., Dehn, J., Rothery, D.A., Calvari, S., 2007. Strombolian explosive styles and source conditions: insights from thermal (FLIR) video. Bull Volcanol 69, 769–784. https://doi.org/10.1007/s00445-006-0107-0
101. Pensa A., Pinton A., Vita L., Bonamico A., De Benedetti A.A., Giordano G. (2019), Atlas of Italian Submarine Volcanic Structures. Mem. Descr. Carta Geol. d'It. 104 (2019): 77 - 183
102. Perona P. and Malik. J. (1990) Scale-space and edge detection using anisotropic diffusion. IEEE Transactions on Pattern Analysis and Machine Intelligence, 12(7):629–639.
103. Petrone, C.M., Mollo, S., Gertisser, R., Buret, Y., Scarlato, P., Del Bello, E., Andronico, D., Ellis, B., Pontesilli, A., De Astis, G., Giacomoni, P.P., Coltorti, M., Reagan, M., 2022. Magma recharge and mush rejuvenation drive paroxysmal activity at Stromboli volcano. Nat Commun 13, 7717. https://doi.org/10.1038/s41467-022-35405-z
104. Phillips, J.C., Woods, A.W., 2001. Bubble plumes generated during recharge of basaltic magma reservoirs. Earth and Planetary Science Letters 186, 297–309. https://doi.org/10.1016/S0012-821X(01)00221-7
105. Pichavant, M., Di Carlo, I., Le Gac, Y., Rotolo, S.G., Scaillet, B., 2009. Experimental Constraints on the Deep Magma Feeding System at Stromboli Volcano, Italy. Journal of Petrology 50, 601–624. https://doi.org/10.1093/petrology/egp014
106. Pichavant, M., Di Carlo, I., Pompilio, M., Le Gall, N., 2022. Timescales and mechanisms of paroxysm initiation at Stromboli volcano, Aeolian Islands, Italy. Bull Volcanol 84, 36. https://doi.org/10.1007/s00445-022-01545-9
107. Pichavant, M., Pompilio, M., D´oriano, C., Dicarlo, I., 2011. Petrography, mineralogy and geochemistry of a primitive pumice from Stromboli: implications for the deep feeding system. ejm 23, 499–517. https://doi.org/10.1127/0935-1221/2011/0023-2109
108. Pioli, L., Erlund, E., Johnson, E., Cashman, K., Wallace, P., Rosi, M., Delgado Granados, H., 2008. Explosive dynamics of violent Strombolian eruptions: The eruption of Parícutin Volcano 1943–1952 (Mexico). Earth and Planetary Science Letters 271, 359–368. https://doi.org/10.1016/j.epsl.2008.04.026
109. Pioli, L., Pistolesi, M., & Rosi, M. (2014). Transient explosions at open-vent volcanoes: the case of Stromboli (Italy). Geology, 42(10), 863-866.
110. Pistolesi, M., Delle Donne, D., Pioli, L., Rosi, M., Ripepe, M., 2011. The 15 March 2007 explosive crisis at Stromboli volcano, Italy: Assessing physical parameters through a multidisciplinary approach. J. Geophys. Res. 116, B12206. https://doi.org/10.1029/2011JB008527
111. Pistolesi, M., Rosi, M., Pioli, L., Renzulli, A., Bertagnini, A., Andronico, D., 2008. The Paroxysmal Event and Its Deposits, in: Calvari, S., Inguaggiato, S., Puglisi, G., Ripepe, M., Rosi, M. (Eds.), Geophysical Monograph Series. American Geophysical Union, Washington, D. C., pp. 317–329. https://doi.org/10.1029/182GM26

112. Polacci, M., Arzilli, F., La Spina, G., Le Gall, N., Cai, B., Hartley, M.E., Di Genova, D., Vo, N.T., Nonni, S., Atwood, R.C., Llewellin, E.W., Lee, P.D., Burton, M.R., 2018. Crystallisation in basaltic magmas revealed via in situ 4D synchrotron X-ray microtomography. Sci Rep 8, 8377. https://doi.org/10.1038/s41598-018-26644-6
113. Polacci, M., Baker, D.R., Bai, L., Mancini, L., 2008. Large vesicles record pathways of degassing at basaltic volcanoes. Bull Volcanol 70, 1023–1029. https://doi.org/10.1007/s00445-007-0184-8
114. Polacci, M., Corsaro, R.A., Andronico, D., 2006. Coupled textural and compositional characterization of basaltic scoria: Insights into the transition from Strombolian to fire fountain activity at Mount Etna, Italy. Geol 34, 201. https://doi.org/10.1130/G22318.1
115. Ripepe, M., Harris, A.J.L., 2008. Dynamics of the 5 April 2003 explosive paroxysm observed at Stromboli by a near-vent thermal, seismic and infrasonic array. Geophysical Research Letters 35, 2007GL032533. https://doi.org/10.1029/2007GL032533
116. Ripepe, M., Lacanna, G., Pistolesi, M., Silengo, M.C., Aiuppa, A., Laiolo, M., Massimetti, F., Innocenti, L., Della Schiava, M., Bitetto, M., La Monica, F.P., Nishimura, T., Rosi, M., Mangione, D., Ricciardi, A., Genco, R., Coppola, D., Marchetti, E., Delle Donne, D., 2021. Ground deformation reveals the scale-invariant conduit dynamics driving explosive basaltic eruptions. Nat Commun 12, 1683. https://doi.org/10.1038/s41467-021-21722-2
117. Ripepe, M., Rossi, M., Saccorotti, G., 1993. Image processing of explosive activity at Stromboli. Journal of Volcanology and Geothermal Research 54, 335–351. https://doi.org/10.1016/0377-0273(93)90071-X
118. Ripepe, M., & Lacanna, G. (2024). Volcano generated tsunami recorded in the near source. Nature Communications, 15(1), 1802.
119. Rizzo, A. L., Federico, C., Inguaggiato, S., Sollami, A., Tantillo, M., Vita, F., ... & Liuzzo, M. (2015). The 2014 effusive eruption at Stromboli volcano (Italy): Inferences from soil CO2 flux and 3He/4He ratio in thermal waters. *Geophysical Research Letters*, *42*(7), 2235-2243.
120. Rosi, M., Bertagnini, A., Harris, A.J.L., Pioli, L., Pistolesi, M., Ripepe, M., 2006. A case history of paroxysmal explosion at Stromboli: Timing and dynamics of the April 5, 2003 event. Earth and Planetary Science Letters 243, 594–606. https://doi.org/10.1016/j.epsl.2006.01.035
121. Rust, A.C., Cashman, K.V., 2004. Permeability of vesicular silicic magma: inertial and hysteresis effects. Earth and Planetary Science Letters 228, 93–107. https://doi.org/10.1016/j.epsl.2004.09.025
122. Sable, J.E., Houghton, B.F., Del Carlo, P., Coltelli, M., 2006. Changing conditions of magma ascent and fragmentation during the Etna 122 BC basaltic Plinian eruption: Evidence from clast microtextures. Journal of Volcanology and Geothermal Research 158, 333–354. https://doi.org/10.1016/j.jvolgeores.2006.07.006
123. Scarani, A., Zandonà, A., Di Fiore, F., Valdivia, P., Putra, R., Miyajima, N., Bornhöft, H., Vona, A., Deubener, J., Romano, C., Di Genova, D., 2022. A chemical threshold controls nanocrystallization and degassing behaviour in basalt magmas. Commun Earth Environ 3, 284. https://doi.org/10.1038/s43247-022-00615-2

124. Self, S., Wilson, L., Nairn, I.A., 1978. Vulcanian eruption mechanisms. Nature 277, 440–443. https://doi.org/10.1038/277440a0
125. Shea, T., 2017. Bubble nucleation in magmas: A dominantly heterogeneous process? Journal of Volcanology and Geothermal Research 343, 155–170. https://doi.org/10.1016/j.jvolgeores.2017.06.025
126. Shea, T., Houghton, B.F., Gurioli, L., Cashman, K.V., Hammer, J.E., Hobden, B.J., 2010. Textural studies of vesicles in volcanic rocks: An integrated methodology. Journal of Volcanology and Geothermal Research 190, 271–289. https://doi.org/10.1016/j.jvolgeores.2009.12.003
127. Spampinato, L., Sciotto, M., Cannata, A., Cannavò, F., La Spina, A., Palano, M., Salerno, G.G., Privitera, E., Caltabiano, T., 2015. Multiparametric study of the F ebruary– A pril 2013 paroxysmal phase of M t. E tna N ew South- E ast crater. Geochem Geophys Geosyst 16, 1932–1949. https://doi.org/10.1002/2015GC005795
128. Stix, J., Torres, R. C., Narváez, L., Raigosa, J. A., Gómez, D., & Castonguay, R. (1997). A model of vulcanian eruptions at Galeras volcano, Colombia. *Journal of Volcanology and Geothermal Research*, *77*(1-4), 285-303.
129. Taddeucci, J., Edmonds, M., Houghton, B., James, M.R., Vergniolle, S., 2015. Hawaiian and Strombolian Eruptions, in: The Encyclopedia of Volcanoes. Elsevier, pp. 485–503. https://doi.org/10.1016/B978-0-12-385938-9.00027-4
130. Taddeucci, J., Pompilio, M., Scarlato, P., 2004. Conduit processes during the July–August 2001 explosive activity of Mt. Etna (Italy): inferences from glass chemistry and crystal size distribution of ash particles. Journal of Volcanology and Geothermal Research 137, 33–54. https://doi.org/10.1016/j.jvolgeores.2004.05.011
131. Toramaru, A., 1990. Measurement of bubble size distributions in vesiculated rocks with implications for quantitative estimation of eruption processes. Journal of Volcanology and Geothermal Research 43, 71–90. https://doi.org/10.1016/0377-0273(90)90045-H
132. Toramaru, A., 2006. BND (bubble number density) decompression rate meter for explosive volcanic eruptions. Journal of Volcanology and Geothermal Research 154, 303–316. https://doi.org/10.1016/j.jvolgeores.2006.03.027
133. Toramaru, A. (2014). On the second nucleation of bubbles in magmas under sudden decompression. Earth and Planetary Science Letters, 404, 190-199.
134. Turchi, A., Di Traglia, F., Luti, T., Olori, D., Zetti, I., & Fanti, R. (2020). Environmental aftermath of the 2019 Stromboli eruption. *Remote Sensing*, *12*(6), 994.
135. Valdivia, P., Marshall, A.A., Brand, B.D., Manga, M., Huber, C., 2022. Mafic explosive volcanism at Llaima Volcano: 3D x-ray microtomography reconstruction of pyroclasts to constrain shallow conduit processes. Bull Volcanol 84, 2. https://doi.org/10.1007/s00445-021-01514-8
136. Turcotte, D. L., Ockendon, H., Ockendon, J. R., & Cowley, S. J. (1990). A mathematical model of vulcanian eruptions. *Geophysical Journal International*, *103*(1), 211-217.
137. Valdivia, P., Zandonà, A., Kurnosov, A., Ballaran, T.B., Deubener, J., Di Genova, D., 2023. Are volcanic melts less viscous than we thought? The case of Stromboli basalt. Contrib Mineral Petrol 178, 45. https://doi.org/10.1007/s00410-023-02024-w
138. Vergniolle, S., Gaudemer, Y., 2015. From Reservoirs and Conduits to the Surface: Review of Role of Bubbles in Driving Basaltic Eruptions, in: Carey, R., Cayol, V.,

Poland, M., Weis, D. (Eds.), Geophysical Monograph Series. Wiley, pp. 289–321. https://doi.org/10.1002/9781118872079.ch14

139. Vezzoli, L., Corazzato, C., 2016. Geological constraints of a structural model of sector collapse at Stromboli volcano, Italy: Sector Collapse Model at Stromboli. Tectonics 35, 2070–2081. https://doi.org/10.1002/2016TC004143
140. Viccaro, M., Cannata, A., Cannavò, F., De Rosa, R., Giuffrida, M., Nicotra, E., Petrelli, M., Sacco, G., 2021. Shallow conduit dynamics fuel the unexpected paroxysms of Stromboli volcano during the summer 2019. Sci Rep 11, 266. https://doi.org/10.1038/s41598-020-79558-7
141. Viccaro, M., Garozzo, I., Cannata, A., Di Grazia, G., Gresta, S., 2014. Gas burst vs. gas-rich magma recharge: A multidisciplinary study to reveal factors controlling triggering of the recent paroxysmal eruptions at Mt. Etna. Journal of Volcanology and Geothermal Research 278–279, 1–13. https://doi.org/10.1016/j.jvolgeores.2014.04.001
142. Visalli, R., Giuffrida, M., Viccaro, M., 2023. Unraveling Textural and Chemical Features in Volcanic Rocks Through Advanced Image Processing: A Case Study From the 2019 Paroxysmal Eruptions of Stromboli. Geochem Geophys Geosyst 24, e2022GC010774. https://doi.org/10.1029/2022GC010774
143. Vona, A., Romano, C., Dingwell, D.B., Giordano, D., 2011. The rheology of crystal-bearing basaltic magmas from Stromboli and Etna. Geochimica et Cosmochimica Acta 75, 3214–3236. https://doi.org/10.1016/j.gca.2011.03.031
144. Woods, A.W., Cardoso, S.S.S., 1997. Triggering basaltic volcanic eruptions by bubble-melt separation. Nature 385, 518–520. https://doi.org/10.1038/385518a0
145. Zhang, Y., Ni, H., Chen, Y., 2010. Diffusion Data in Silicate Melts. Reviews in Mineralogy and Geochemistry 72, 311–408. https://doi.org/10.2138/rmg.2010.72.8